doi.org/10.26434/chemrxiv.13735084.v7

Unimolecular, bimolecular and intramolecular hydrolysis mechanisms of 4-nitrophenyl β-D-glucopyranoside

Amani Alhifthi, Spencer Williams

Submitted date: 12/04/2021 • Posted date: 12/04/2021

Citation information: Alhifthi, Amani; Williams, Spencer (2021): Unimolecular, bimolecular and intramolecular hydrolysis mechanisms of 4-nitrophenyl β-D-glucopyranoside. ChemRxiv. Preprint. https://doi.org/10.26434/chemrxiv.13735084.v7

1,2-trans-Glycosides hydrolyze through different mechanisms at different pH values, but systematic studies are lacking. Here we report the pH-rate constant profile for the hydrolysis of 4-nitrophenyl β-D-glucoside. An inverse kinetic isotope effect of $k(H_3O^+)/k(D_3O)^+ = 0.65$ in the acidic region indicates that the mechanism requires the formation of the conjugate acid of the substrate for the reaction to proceed, with heterolytic cleavage of the glycosidic C-O bond. Reactions in the pH-independent region exhibit general catalysis with a single proton in flight, a normal solvent isotope effect of $k_H/k_D = 1.5$, and when extrapolated to zero buffer concentration show a small solvent isotope effect $k(H_2O)/k(D_2O) = 1.1$, consistent with water attack through a dissociative mechanism. In the basic region, solvolysis in ^{18}O-labelled water and H_2O/MeOH mixtures allowed detection of bimolecular hydrolysis and neighboring group participation, with a minor contribution of nucleophilic aromatic substitution. Under mildly basic conditions, a bimolecular concerted mechanism is implicated through an inverse solvent isotope effect of $k(HO^-)/k(DO^-) = 0.5$ and a strongly negative entropy of activation ($DS^‡ = -13.6$ cal mol^{-1} K^{-1}). Finally, at high pH, an inverse solvent isotope effect of $k(HO^-)/k(DO^-) = 0.6$ indicates that the formation of 1,2-anhydrosugar is the rate determining step.

File list (2)

manuscript_120421.docx (425.84 KiB)	view on ChemRxiv • download file
SI_120421.docx (1.09 MiB)	view on ChemRxiv • download file

Unimolecular, bimolecular and intramolecular hydrolysis mechanisms of 4-nitrophenyl β-D-glucopyranoside

Amani Alhifthi and Spencer J. Williams*

School of Chemistry and Bio21 Molecular Science and Biotechnology Institute, University of Melbourne, Parkville 3010, Victoria, Australia

sjwill@unimelb.edu.au

Keywords: carbohydrates, neighboring group participation, solvent isotope effect, glycoside

Abstract. 1,2-*trans*-Glycosides hydrolyze through different mechanisms at different pH values, but systematic studies are lacking. Here we report the pH-rate constant profile for the hydrolysis of 4-nitrophenyl β-D-glucoside. An inverse kinetic isotope effect of $k(H_3O^+)/k(D_3O^+) = 0.65$ in the acidic region indicates that the mechanism requires the formation of the conjugate acid of the substrate for the reaction to proceed, with heterolytic cleavage of the glycosidic C-O bond. Reactions in the pH-independent region exhibit general catalysis with a single proton in flight, a normal solvent isotope effect of $k_H/k_D = 1.5$, and when extrapolated to zero buffer concentration show a small solvent isotope effect $k(H_2O)/k(D_2O) = 1.1$, consistent with water attack through a dissociative mechanism. In the basic region, solvolysis in ^{18}O-labelled water and H_2O/MeOH mixtures allowed detection of bimolecular hydrolysis and neighboring group participation, with a minor contribution of nucleophilic aromatic substitution. Under mildly basic conditions, a bimolecular concerted mechanism is implicated through an inverse solvent isotope effect of $k(HO^-)/k(DO^-) = 0.5$ and a strongly negative entropy of activation ($\Delta S^{\ddagger} = -13.6$ cal mol^{-1} K^{-1}). Finally, at high pH, an inverse solvent isotope effect of $k(HO^-)/k(DO^-) = 0.5$ indicates that the formation of 1,2-anhydrosugar is the rate determining step.

Introduction

Carbohydrates are the most abundant polymer of biological origin on earth. Accordingly, the mechanism of their hydrolysis is of enduring interest. As a result of the powerful charge stabilization effects of the endocyclic oxygen on positive charge development at the anomeric carbon, an oxocarbenium ion intermediate or oxocarbenium-ion-like transition state feature extensively in almost all transformations at the anomeric centre.[1] The lifetime of the glucopyranosyl cation in water is short and is estimated at 1-3 ps.[2, 3] As a consequence, nucleophilic substitution reactions of hydroxylated glycosides tend to straddle the border of S_N1 and S_N2 reactions. The hydrolysis (or solvolysis) of glycosides of simple (alkyl) alcohols has been extensively studied,[4] as have other simple leaving groups such as azide (glycosyl azides),[2] fluoride (glycosyl fluorides)[5-7] or neutral amines (glycosyl pyridinium ions).[3, 5, 8]

The non-enzymatic hydrolysis reactions of aryl glycosides are less well studied, which is surprising as these compounds are widely used substrates for the study of glycosidases, nature's catalysts for glycoside hydrolysis. Under acid-catalyzed conditions,[9] hydrolysis involves heterolysis of the glycosidic bond,[10] through a specific acid catalyzed process with an oxygen-18 kinetic isotope effect for 4-nitrophenyl β-D-(1-^{18}O)-glucopyranoside of k_{16}/k_{18} = 1.036 ± 0.002.[11] Aryl glycosides are hydrolysed more rapidly than alkyl glycosides,[10, 12] which is consistent with their better leaving group ability. Under identical acidic conditions, phenyl α-D-glucoside is hydrolyzed approximately 50-fold faster than methyl α-D-glucopyranoside; the rate ratio is about 8-fold for the β-series.[10] Hammett reaction constants of ρ = –0.006 and –0.66 have been reported for acidic hydrolysis of aryl α- and β-D-glucopyranosides, respectively.[13, 14]

Under neutral conditions, methyl β-glucopyranoside hydrolyses with a rate constant of 4.7×10^{-15} s^{-1} at 25 ºC,[15] while 2,4-dinitrophenyl β-glucoside (DNPGlc) hydrolyses with a rate constant of 5.58×10^{-6} s^{-1} at 37 ºC,[16] showing that a highly activated 2,4-dinitrophenoxide group confers significantly greater reactivity. The entropy of activation ($\Delta S^{\ddagger}$) for these two processes are –24 cal mol^{-1} K^{-1} (at 25 ºC) and 33.8 cal mol^{-1} K^{-1} (at 37 ºC), respectively, suggesting that the uncatalyzed hydrolysis of methyl β-glucopyranoside involves a bimolecular process with significant participation by the nucleophile,[15] while that of DNPGlc involves a more dissociative (ionic) process, possibly involving a short-lived oxocarbenium ion intermediate.[16] Jencks reported a solvent kinetic isotope effect for the hydrolysis of α-glucopyranosyl fluoride in the pH independent region of k_H/k_D = 0.9.[7] As this

value is close to unity it shows limited fractionation and, like the hydrolysis of DNPGlc, is consistent with a dissociative mechanism for this substrate bearing a good leaving group.

Under basic conditions hydrolysis of aryl glycosides also involves cleavage of the glycosidic bond.[17] Interestingly, 4-nitrophenyl β-glucoside (PNPGlc) is hydrolyzed 195-fold faster in 0.1 N NaOH than in 0.1 N HCl (both at 65 ºC).[18] The oxygen-18 kinetic isotope effect for hydrolysis of 4-nitrophenyl β-D-(1-^{18}O)-galactopyranoside, k_{16}/k_{18} = 1.029 ± 0.002 indicates a transition state with substantial carbon-oxygen bond cleavage.[11] Alkaline solvolysis reactions exhibit sharp sensitivity to substituent effects with Hammett reaction constants of ρ = +2.8-4.0[14] and +2.48-2.5[13, 19] aryl α- and β-D-glucopyranosides, respectively. These effects mean that while 4-nitrophenyl α-D-glucopyranoside hydrolyses at approximately the same rate as the unsubstituted phenyl analogue under acidic conditions, under strongly basic conditions (3.9 N NaOH) it hydrolyses approximately 300,000-fold faster than the phenyl analogue.[14] Under basic conditions, phenyl β-D-glucopyranoside hydrolyses several orders of magnitude faster than phenyl α-D-glucopyranoside,[13, 14] and there is compelling evidence for neighboring group participation in the basic solvolysis of aryl β-D-glucopyranosides involving a C2-oxyanion and proceeding through a 1,2-anhydro sugar.[17, 19] This includes substitution with retention of anomeric configuration when using methoxide,[20] and the rate retardation induced by blocking the C2 oxygen with a methyl group.[21, 22] For the related reaction of 4-nitrophenyl α-D-mannopyranoside (which shares a 1,2-*trans* relationship),[22] the carbon-13 kinetic isotope effect (KIE) for C1 is 1.026 ± 0.006,[23] which is in agreement with an S_N2 reactions on glycosides,[24] and the ratio of k_L/k_H >1 indicates a concerted rather than dissociative mechanism. The oxygen-18 KIE for the C2-oxygen is greater than unity (1.044 ± 0.0060), implicating its direct involvement in the reaction.[23]

Here we report the pH-rate constant profile of the hydrolysis of PNPGlc. We distinguish four main mechanistic regimes and six contributing reaction mechanisms (**Figure 1**). By exploration of buffer and solvent isotope effects, we show that PNPGlc undergoes specific acid catalyzed hydrolysis at low pH, and uncatalyzed hydrolysis in the pH independent region when buffer concentration was extrapolated to zero. At high pH two main mechanisms are observed: a bimolecular nucleophilic substitution under mildly basic conditions, and neighbouring group participation by the C2-oxyanion via a 1,2-anhydro sugar intermediate under strongly basic conditions.

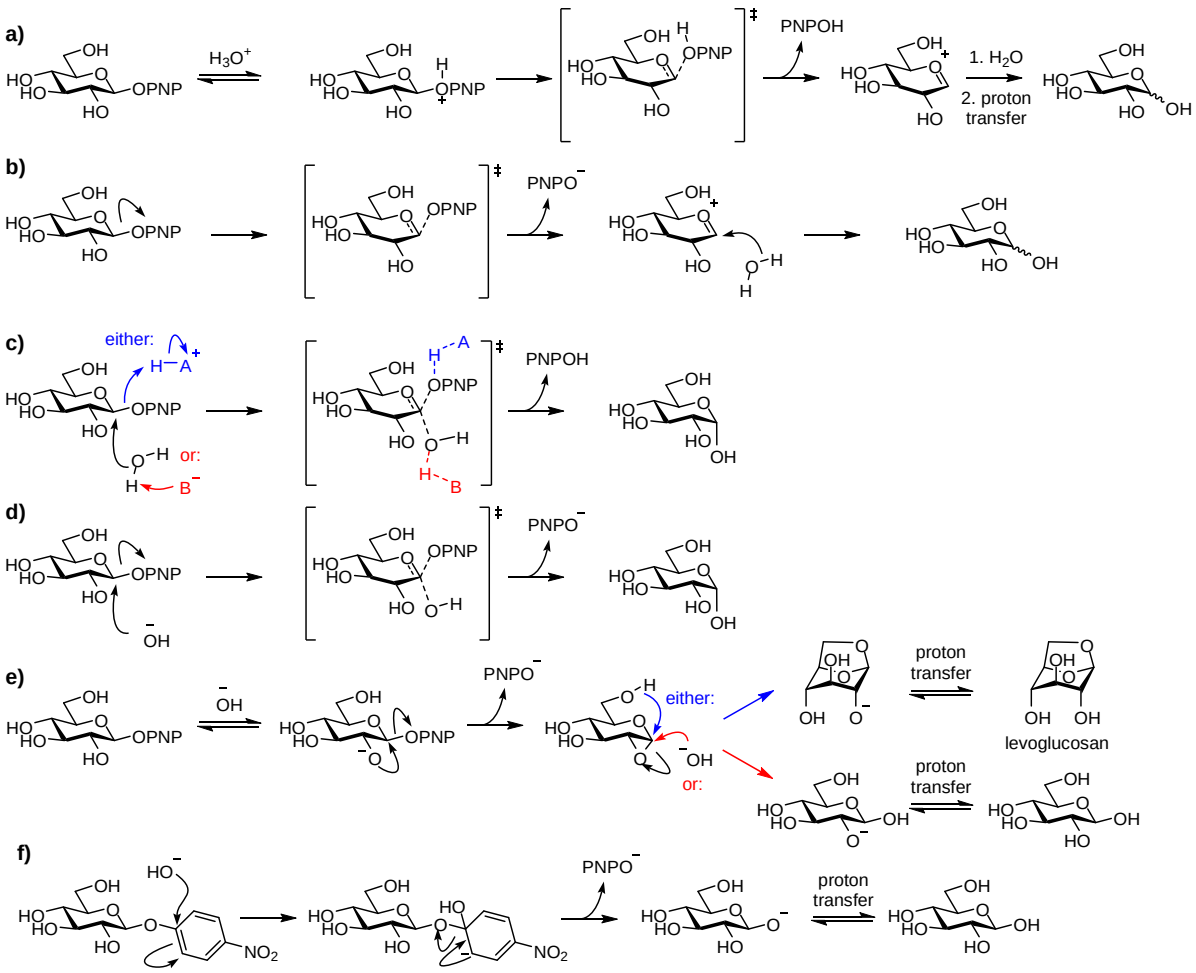

Fig. 1. Mechanisms of hydrolysis of PNPGlc: (a) specific acid catalyzed (unimolecular); (b) uncatalyzed dissociative; (c) general acid/base catalyzed; (d) biomolecular base-promoted; (e) neighboring group participation by C2-oxyanion; (f) nucleophilic aromatic substitution.

Results

1. pH-rate constant profile for formation of 4-nitrophenol/phenolate from PNPGlc

Reactions were conducted at elevated temperature, typically 90 °C, by monitoring formation of the 4-nitrophenol/phenolate anion either in real time in a cuvette using a spectrophotometer, or for slower reactions in sealed Wheaton vials after quenching with base. At the extremes of pH reaction rates were too fast at 90 °C to be accurately determined. In these cases, reactions were conducted at lower temperature and Arrhenius plots were used to extrapolate rates to 90 °C. pH values of solutions and buffers at elevated temperature were calculated from pH measured at 25 °C using the temperature sensitivity coefficients of the pK_a values of H_2O or of buffers. Reactions were performed in 2 M NaCl solution and rates corrected for salt effects by varying salt concentration from 0.25-2 M and extrapolating to zero salt concentration (**Tables S3**, **S4, S5; Fig. S3, S4**). In the pH independent and weakly basic regions rates buffer effects were measured by varying the buffer concentration from 0.25-1 M and extrapolating to zero buffer concentration (**Table S6, S7; Fig. S5, S6**).

The experimentally determined pH-rate constant profile, log *k* versus pH, for hydrolysis of PNPGlc at 90 °C is corrected for buffer and salt effects, and for the strongly basic region, a minor incursion of nucleophilic aromatic substitution (**Table 1**, **Fig. 2**). The plot reveals four distinct regions: the acidic region (pH –1 to 0), a pH-independent region (pH 1 to 7), and two basic regions (pH 8 to 10 and 10 to 12). The overall rate law is given by equation 1:

$$k_{obs} = k_H[H^+] + k_{uncat} + k_{OH}[HO^-] + k_{NGP} \qquad \text{eq. 1}$$

where k_H is the rate constant for the specific acid catalyzed reaction, k_{uncat} is the rate constant for the uncatalyzed reaction, k_{OH} is the rate constant for the bimolecular reaction involving hydroxide, and k_{NGP} is the rate constant for neighboring group participation by C2-oxyanion. In each region the slope of the line of best fit corresponds to the kinetic order in hydronium or hydroxide.[25, 26]

Table 1. Rates for the hydrolysis of PNPGlc (*k*) at 90 ºC, with pH corrected for 90 °C. Observed rates (k_{obs}) are corrected as followed. All rates are extrapolated to [salt] = 0. Rates in the region pH 3.8-7.8 were extrapolated to [buffer] = 0. Rates in the strongly basic region were corrected for bimolecular, and nucleophilic aromatic substitution processes (see **Table S11**).

pH	k_{obs} (y x 10^2) min^{-1}	Correction factor	*k* (y x 10^2) min^{-1}	r^2	Δy [a]	log *k*
–1	1.5	0.42 [b]	0.630	0.99	0.017	–2.2
–0.58	0.23	0.42 [b]	0.1	0.99	0.01	–3
0.42	0.023	0.42 [b]	0.01	0.99	0.04	–4
1.42	0.011	0.42 [b]	0.005	0.99	0.13	–4.3
3.8	0.016	0.25 [c]	0.004	0.99	0.25	–4.41
4.8	0.01	0.25 [c]	0.0025	0.99	0.25	–4.60
5.8	0.0112	0.25 [c]	0.0025	0.99	0.25	–4.60
6.8	0.0124	0.25 [c]	0.0031	0.99	0.070	–4.6
7.8	0.006	1 [d]	0.0063	0.97	0.23	–4.22
8.26	0.065	1 [d]	0.060	0.99	0.22	–3.22
8.55	0.30	1 [d]	0.60	0.98	0.4	–2.20
9.55	6.00	1 [d]	6.00	0.98	0.051	–1.20
10.42	50.60	0.89 [e]	45	0.98	0.25	–0.34
11.42	50.60	0.89 [e]	45	0.98	0.24	–0.30
12.42	56.17	0.89 [e]	50	0.94	0.2	–0.30

[a] Relative error = Δy = (y`/y), standard error = y`. [b] Correction factor = salt effect. [c] Correction factor = buffer effect. [d] No correction factor. [e] Correction factor = 1 – contribution of bimolecular process – contribution of nucleophilic aromatic substitution = 1 – 0.1 – 0.01.

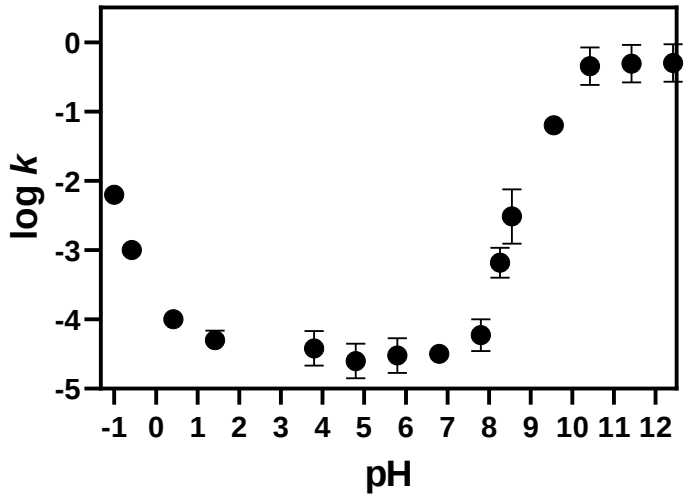

Fig. 2. pH-rate constant profile for hydrolysis of PNPGlc, corrected for pH at 90 °C. k_H = 2.90 × 10^{-3} M^{-1} min^{-1}, k_{uncat} = 3.77 × 10^{-5} min^{-1}, k_{OH} = 5.82 × 10^{-2} M^{-1} min^{-1}, k_{NGP} = 0.27 min^{-1} (for rate data, see **Table 1**).

2. Mechanism of hydrolysis in the acidic region

Overend and co-workers noted that for the hydrolysis of PNPGlc in 2 N hydrochloric acid at 72 °C, 5-10% of a disaccharide product is formed, and inclusion of D-glucose in the reaction mixtures did not affect measured rates, indicating that disaccharide formation resulted from condensation of glucose released in the reaction.[12] Here, ^{1}H NMR analysis of the reaction mixture obtained from the reaction of PNPGlc (50 mM) at pH –0.8 (corrected from pH 0.5 measured at room temperature) at 50% completion revealed exclusive formation of only PNPOH and glucose (**Figure S11**), and thus rates measured from quantifying production of PNPOH/$PNPO^-$ reflect exclusively hydrolysis.

Arrhenius activation parameters were calculated for the hydrolysis reaction in the acidic region. The rate of the hydrolysis of 0.1 mM PNPGlc in 2 M NaCl was measured at four different temperatures in 0.26 M HCl (**Table S8**, **Figure S7a**). Plotting log k_{obs} as a function of the inverse of temperature yielded the activation energy (E_a), the pre-exponential factor (ln A), and allowed calculation of thermodynamic factors, the entropy of activation ($\Delta S^{\ddagger}$) and enthalpy of activation ($\Delta H^{\ddagger}$) (**Table 2**). Because reactions at low pH involve pre-equilibria, the measured rate constants are composites of the equilibrium constant and the rate of the irreversible chemical step, and give rise to apparent thermodynamic parameters.

Table 2. Arrhenius parameters for hydrolysis of PNPGlc.

pH [a]	E_a (kcal mol^{-1})	ln A	$\Delta S^{\ddagger}$ [a] (cal mol^{-1} K^{-1})	$\Delta H^{\ddagger}$ (kcal mol^{-1})
0.58	25.2±0.1 [b]	29.8±0.1 [b]	0.73±0.07 [b]	24.6±0.1 [b]
6	29.0±0.01	31.0±0.02	3.07±0.02	28.4±0.01
9.5	21.3±0.1	22.6±0.1	–13.6±0.1	20.7±0.1
14	20.4±0.1 [b]	27.4±0.1 [b]	–3.9±0.1 [b]	19.7±0.1 [b]

[a] at 298.1 K, [b] apparent thermodynamic parameters.

To investigate whether there is a salt effect, a series of reactions were conducted at pH 0 and varying the concentration of NaCl from 0.25-2 M (**Table S3; Figure S3a**). A plot of the measured rates gave a straight line with slope 0.00012 min^{-1} M^{-1}, indicating a primary kinetic salt effect and allowing extrapolation to [salt] = 0 where k = 0.00015 min^{-1} (**Figure S4a**).

The solvent isotope effect at pH –0.75 was measured in solutions containing [H_3O^+] = 1 M or [D_3O^+] = 1 M and [NaCl] = 150 mM, [S] = 0.1 mM at 75 °C. The measured rates were $k(D_3O^+)$ = (3.2±0.01) × 10^{-3} min^{-1} and $k(H_3O^+)$ = (2.02±0.04) × 10^{-3} min^{-1}, giving a solvent isotope effect of $k(H_3O^+)/k(D_3O^+)$ = 0.65±0.01 (**Table S12; Figure S9a**). Using the method of fractionation factors,[27] the calculated solvent isotope effect for the specific acid catalyzed process, φ^R/φ^P = 0.476 (**Table S13**).

3. Mechanism of hydrolysis in the pH-independent region

Rates measured for reactions in the pH independent region (pH 3.8-6.8, using phosphate/citrate or phosphate buffer in 2 M NaCl) of the pH-rate profile give a line of best fit with a slope of essentially zero (**Figure 2**). Reaction rates in this region therefore have close to zero dependency on [H^+], and in this range may occur through uncatalysed hydrolysis (k_{uncat}), or mechanisms involving general acid/base catalysis, nucleophilic participation by buffer (k_{buffer}) or salt effects (k_{salt}). The empirical rate law that fits this analysis is equation 2:

$$k_{obs} = k_{uncat} + k_{buffer}[\text{buffer}] + k_{salt}[\text{salt}] \qquad \text{eq. 2}$$

Initially, we analysed the products of the reaction in the presence of NaCl, KCl and $NaClO_4$ to ensure that measured rates are for hydrolysis. ^{1}H NMR spectroscopy revealed only the formation of glucose and 4-nitrophenol (for product analysis with $NaClO_4$, see **Figure S12**). To assess whether NaCl participates in the reaction, we first examined the effect of changing [NaCl]. The plot of [NaCl] versus rate was almost flat, with slope = (5.2 ± 1.1) ×

10^{-6} M^{-1} min^{-1}, indicating essentially no salt effect (**Table S4, Figure S4b**). Next, we independently varied the cation (to KCl) and anion (to $NaClO_4$) and examined the effects upon reaction rates. At 2 M salt, the rate decreased (1.5 ± 0.2)-fold in KCl versus NaCl, and by (2.0 ± 0.2)-fold in $NaClO_4$, indicating limited salt participation, even at high concentrations with slope = 0. Variation of [buffer] under conditions of pseudo constant ionic strength, in this case with [NaCl] = 2 M at pH 3.8, gave a plot with slope k_{buffer} = 5.11 × 10^{-5} M^{-1} min^{-1} (**Table S6**, **Figure S5d**).

Collectively, the above experiments define k_{buffer} and k_{salt}, allowing calculation of the rate constant for the uncatalyzed hydrolysis reaction (k_{uncat}), the thermodynamic parameters (at pH 5.8; **Table S8**; **Fig. S7, S8**; **Table 2**), and the solvent isotope effect. The solvent isotope effect for the uncatalyzed reaction was measured in H_2O or D_2O solvent, pH = pD = 6.8, with [NaCl] = 150 mM and [buffer] = 0.005 M. The measured rates were: $k_{uncat}(D_2O)$ = (3.02±0.17) × 10^{-5} min^{-1} and $k_{uncat}(H_2O)$ = (3.40±0.25) × 10^{-5} min^{-1} (**Table S12; Figure S9b**), giving a solvent isotope effect of $k_{uncat}(H_2O)/k_{uncat}(D_2O)$ = 1.1±0.1.

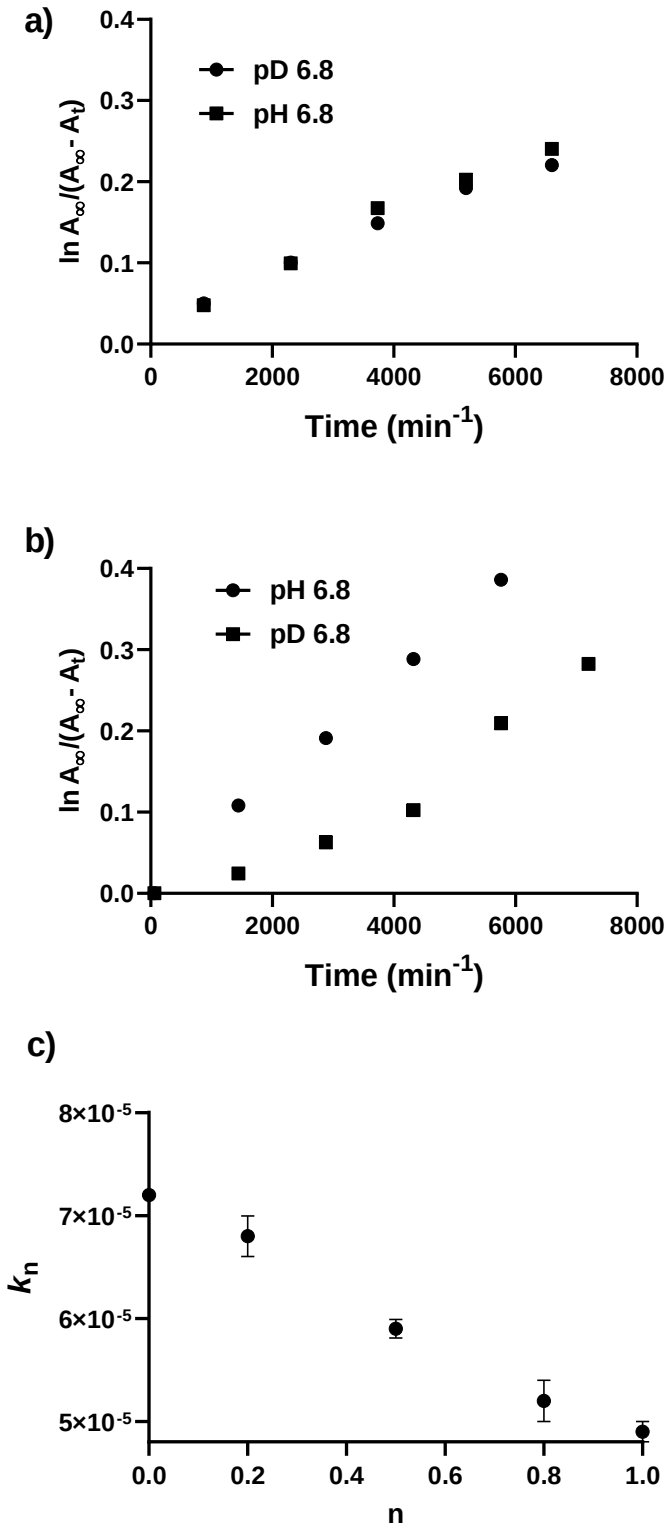

Fig. 3. Reactions in the pH independent region (pH = 6.8) at 90 °C. (a) Solvent isotope effect at [buffer] = 0.005 M. (b) Solvent isotope effect for [buffer] = 1 M. (c) Proton inventory plot of k_n as a function of D_2O fraction (n) at [buffer] = 1 M, p(H,D) 6.8.

To study the nature of the buffer effect, we initially tested for general acid/base catalysis by measuring a solvent isotope effect for [buffer] = 1 M in H_2O and D_2O at pH 3.8. Solvent isotope effects allow detection of general acid/base catalysis by measuring the number of protons in flight in the rate determining step. The solvent isotope effect, k_H/k_D = 1.5 ± 0.1, which indicates general acid/base catalysis (**Table S12**, **Fig. S9**). While this solvent isotope effect gives evidence for general acid/base catalysis, it does not rule out nucleophilic participation by buffer. To establish whether phosphate or citrate in the buffer participates in the reaction, we repeated the pH 3.8 rate measurements in 1 M acetate buffer (with 2 M NaCl) at the same pH and observed no significant difference in rates. However, this data does not allow clear conclusions to be drawn as the pK_a values for acetic acid (pK_a 4.75) and citric acid (pK_{a2} 4.75) are similar,[28] and they may engage in nucleophilic participation to similar degrees. Attempts to detect the formation of a glycosyl acetate by NMR analysis of the product mixture were unsuccessful, but the failure to observe this species is inconclusive for nucleophilic participation.

We next sought to determine the number of protons in flight in the transition state of the reaction in buffer in which general catalysis is implicated. The proton inventory technique is a solvent isotope-effect experiment that gives information about the number of protons transferred in a chemical reaction.[29] Measurements are made of the solvent isotope effect in varying mixtures of light and heavy solvent. If the proton inventory plot is linear, only one proton is involved in the reaction, and if the proton inventory is curved, at least two protons are involved.

The solvent isotope effect in 1 M phosphate buffer at 90 °C was k_H/k_D = 1.4 ± 0.09. The inverse solvent isotope effect indicates that the protonation step is involved in the rate determining step and the reaction at high buffer concentration proceeds with general acid/base catalysis. Next, we measured the rate in a 20, 50 and 80% mixtures of light and heavy water in 1 M buffer and 2 M NaCl at 90 °C (**Table S14; Fig. S10**). The measured rate constants for different mixtures of isotopic solvents were plotted against the fraction of deuterium (*n*) and yielded a linear plot (**Fig. 3c**). Because plots of low curvature can be difficult to distinguish from linear plots, this data should be examined at the point of greatest curvature, namely $k_{0.5}$. The observed rate at $k_{0.5}$ = (5.91±0.09) × 10^{-5} is in good agreement with the mean(k_0 and k_1) = (5.98±0.08) × 10^{-5}. Thus, these data suggest that the solvent isotope effect arises from a single hydrogenic site in the transition state; that is, only one proton is undergoing transfer in the rate-determining step (**Fig. 1c**). As the 4-nitrophenolate leaving group can stabilize negative charge, we suggest that the proton in flight is involved in base deprotonation of the water nucleophile.

4. Mechanism of hydrolysis in the basic region

(i) Mechanism under mildly basic conditions

^{1}H NMR analysis of pH 7.8, 8.26 and 8.55 reaction mixtures at 50% completion revealed only substrate, PNPOH/$PNPO^-$, and glucose. In order to determine whether product formation occurred through nucleophilic substitution at C1 or by nucleophilic aromatic substitution, reactions were conducted in $H_2{}^{18}O$ and then analysed by mass spectrometry in negative ion mode. This revealed the presence of $PNPO^-$ as *m*/*z* 138.02, corresponding to the ^{16}O isotopomer, with no detectable ^{18}O-labelled product. Thus, rates measured from quantifying production of $PNPO^-$ reflect only the bimolecular hydrolysis reaction.

To test for buffer participation, we measured rates while varying buffer concentration under conditions of pseudo constant ionic strength, with [NaCl] = 2 M at 90 °C (**Table S7;**

Fig. S6). This gave linear plots with slope of close to zero (pH 7.8, (−¿3 ± 3) × 10^{-6} M^{-1} min^{-1}; pH 8.26, (3.34 ± 0.9) × 10^{-5} M^{-1} min^{-1}; pH 8.55, (4.91 ± 0.16) × 10^{-4} M^{-1} min^{-1}), indicating that the rate of reaction is independent of buffer concentration across this pH range. The salt effect in the weakly basic region was tested by measuring the reaction rate in 1 M NaCl (k = (6.05 ± 0.03) × 10^{-4} min^{-1}) and 0.25 M NaCl (k = (6.5 ± 0.03)× 10^{-4} min^{-1}) at pH 8.26 at 90 °C, indicating that in the weakly basic region there is no significant salt effect (**Fig. S3**).

The above analysis allowed calculation of the thermodynamic parameters for the biomolecular base-promoted hydrolysis reaction (**Table S9**; **Fig. S7, S8; Table 2**). The solvent isotope effect for the biomolecular base-promoted hydrolysis reaction was measured at pD = pH = 9.1 and 90 °C (**Fig. S9**). The measured rates were: $k(DO^-)$ = (1.77±0.16) × 10^{-3} min^{-1} and $k(HO^-)$ = (9.01±0.29) × 10^{-4} min^{-1}, for a solvent isotope effect of $k(HO^-)/k(DO^-)$ = 0.5 ± 0.1 (**Table S12**). The solvent isotope effect for the biomolecular process calculated using solvent isotope fractionation factors is 0.476 (**Table S13**).

(ii) Mechanism under strongly basic conditions

At pH 12.42 and 55 °C, ^{1}H NMR analysis of the product mixture of reactions run to 70% completion revealed $PNPO^-$, and a complex set of peaks assigned as the base-decomposition product of glucose and a new product with a characteristic H1 signal at δ 5.30 ppm in D_2O that was assigned as 1,6-anhydro-β-D-glucopyranose (levoglucosan) (**Fig. S13**). The observation of 1,6-anhydroglucose provides evidence for neighboring group participation involving substitution of the anomeric group by the substrate 2-oxyanion, via a 1,2-anhydro sugar (epoxide) intermediate. However, the 1,2-anhydrosugar intermediate can partition in two ways: either by nucleophilic substitution involving intramolecular reaction with the 6-hydroxyl group (leading to the 1,6-anhydro sugar, which is stable to base), or by reaction with hydroxide (leading to glucose, which decomposes under the basic conditions of the reaction).

In order to determine whether product formation occurred through nucleophilic substitution at C1 or by nucleophilic aromatic substitution, reactions were conducted in $H_2{}^{18}O$ and then analysed by mass spectrometry in negative ion mode. This revealed the presence of $PNPO^-$ as m/z 138.02, corresponding to the ^{16}O isotopomer, and a second peak at m/z 140.02, corresponding to the ^{18}O isotopomer, in a ratio of 99.1:0.89. This data demonstrate that nucleophilic aromatic substitution contributes just under 1% of the rate observed by quantifying production of $PNPO^-$.

To investigate the partitioning of the 1,2-anhydrosugar intermediate between intramolecular substitution and hydroxide substitution, the reaction was repeated in 1:1 MeOH/H_2O with 0.5 M NaOH at 55 °C (pH 12.96). ^{1}H NMR spectroscopy revealed the formation of a mixture of methyl α-D-glucopyranoside, methyl β-D-glucopyranoside and levoglucosan in a ratio of 10:18:72 (**Fig. S14**). As explained earlier, levoglucosan arises through neighboring group participation by a C2-oxyanion, which also produces methyl β-D-glucopyranoside. On the other hand, methyl α-D-glucopyranoside (quantified through integration of the anomeric CH_3 group) arises exclusively by bimolecular substitution. The pK_a value of MeOH is 15.3 at 25 °C. Assuming the temperature dependence of the pK_a of MeOH is similar to that of water (pK_a 13.26), for 1:1 MeOH/H_2O with 0.5 M NaOH the [MeO^-] = 0.02, this allows calculation of the rate of neighboring group participation (formation of levoglucosan and β-D-glucose, which decomposes in base) by subtraction of the rate of bimolecular substitution and nucleophilic aromatic substitution.

Reactions in this region are second order, depending on the concentration of hydroxide and substrate.[19, 22] However, under conditions of excess alkali, the reaction can be treated as first order, dependent only upon the concentration of substrate.[19] To investigate for a salt effect, reactions were studied at 0-1.58 M NaCl (**Table S5**). A plot of k vs NaCl concentration gave a line with slope close to zero showing that there is no significant salt effect in this region and an average rate constant of $k = (41.7 \pm 3.4) \times 10^{-3}$ min^{-1} (**Fig. S4**).

The above data allowed calculation of the thermodynamic parameters for the neighbouring group participation reaction (pH 12.42, **Table S11; Fig. S7, S8; Table 2**), and the solvent isotope effect. Again, as for reactions at low pH, reactions at high pH involve pre-equilibria, and the measured rate constants are composites of the equilibrium constant and the rate of the irreversible chemical step and give rise to apparent thermodynamic parameters. The solvent isotope effect was measured in H_2O or D_2O solvent at pH = pD = 13.1, with [NaOD] = [NaOH] = 1 M and [NaCl] = 150 mM at 55 °C. The measured rates were: $k(DO^-) = (1.0 \pm 0.11) \times 10^{-2}$ min^{-1} and $k(HO^-) = (6.0 \pm 0.9) \times 10^{-3}$ min^{-1}), allowing calculation of a solvent isotope effect of $k(HO^-)/k(DO^-) = 0.6 \pm 0.18$ (**Table S12; Fig. S9**). This is in agreement with the calculated solvent isotope effect (0.56) based on solvent isotope fractionation factors for the intermolecular reaction (**Table S13**).

Discussion

The pH rate profile for PNPGlc hydrolysis (**Fig. 2**) was calculated from the pH rate

profile for formation of PNPOH/$PNPO^-$ by careful measurement of individual contributing reactions and correction for their contribution to the observed rates (**Table 1**). The profile gives evidence for at least 4 mechanistic regimes: at low pH, in the intermediate pH range, in the mildly basic region, and at high pH.

In the acidic region, the pH-rate constant plot is first order in hydronium concentration (slope = –1.21 ± 0.20, k_H = 2.90 × 10^{-3} M^{-1} min^{-1}) the apparent enthalpy of activation ($\Delta H^{\ddagger}$ = 24.6 kcal mol^{-1}) is in good agreement with the value measured by Snyder and Link[18] ($\Delta H^{\ddagger}$ = 25.5 kcal mol^{-1}) under similar first order conditions. The solvent kinetic isotope effect was $k(H_3O^+)/k(D_3O^+)$ = 0.65±0.01. The inverse kinetic isotope effect indicates that there is a greater preference for deuteration (D^+) than protonation of the substrate and that the specific acid catalysed hydrolysis of PNPGlc is a stepwise mechanism. Interpretation of solvent KIEs is complicated by the contributions from primary effects for protons undergoing transfer, and secondary effects, for example because of deuteration at exchangeable positions. Using the method of fractionation factors, and assuming a specific acid catalyzed mechanism, the calculated isotope fractionation factor φ for the hydrolysis of PNPGlc at pD –0.41 at 75 °C was 0.48. Collectively this data is consistent with the reaction mechanism shown in **Fig. 1a**, which involves a specific acid catalysed reaction in which the substrate is converted to its conjugate acid, unimolecular fission to form the oxocarbenium ion, followed by a rate-limiting reaction with H_2O. This data is consistent with observations made for methyl α- and β-glucopyranosides[30] and -xylopyranosides.[4]

In the pH independent region (slope = –0.02 ± 0.04, k_{uncat} = 3.77 × 10^{-5} min^{-1}) there was small solvent isotope effect $k(H_2O)/k(D_2O)$ = 1.1±0.1. This compares favourably with the solvent isotope effect of $k(H_2O)/k(D_2O)$ = 0.93 measured by Banait and Jencks for the hydrolysis of α-glucopyranosyl fluoride at 30 °C in the pH independent region.[7] A positive entropy of activation of $\Delta S^{\ddagger}$ = 3.07 cal mol^{-1} K^{-1} was measured, similar to that for the acidic region, which is again consistent with a unimolecular transition state for the hydrolysis of PNPGlc. Together these data indicate that the uncatalysed hydrolysis of PNPGlc proceeds through a dissociative mechanism to give short-lived glucosyl oxocarbenium ion, followed by nucleophilic attack of water molecule. The positive entropy of activation is inconsistent with a bimolecular process, and the observed solvent KIE is close to unity, which is consistent with a calculated isotope fraction factor of 1 for the dissociative mechanism in **Fig. 1b**. The entropy of activation ($\Delta S^{\ddagger}$ = 3.07 cal mol^{-1} K^{-1}) is positive, but smaller than that measured for the hydrolysis of DNPGlc ($\Delta S^{\ddagger}$ = 33.8 cal mol^{-1} K^{-1}),[16] and distinct from the negative value

measured for hydrolysis of methyl β-glucopyranoside ($\Delta S^{\ddagger}$ = –24 cal mol^{-1} K^{-1}).[15] Extrapolation of the rate for hydrolysis of PNPGlc to ambient temperature, $k_{25°C} = 2.86 \times 10^{-10}$ s^{-1} reveals it is approximately five orders of magnitude faster than that for hydrolysis of methyl β-glucopyranoside $k_{25°C} = 1.9 \times 10^{-15}$ s^{-1}.[15]

Under weakly basic conditions the pH-rate constant plot is approximately first order in hydroxide (slope = 1.5 ± 0.2, $k_{OH} = 5.82 \times 10^{-2}$ M^{-1} min^{-1}), and had a solvent isotope effect of 0.5±0.1, which compares favourably to the solvent isotope effect of 0.66 reported by Banait and Jencks for the hydroxide mediated hydrolysis of α-glucopyranosyl fluoride at 30 °C.[7] In this region the reaction had a strongly negative entropy of activation ($\Delta S^{\ddagger}$ = –13.6 cal mol^{-1} K^{-1}) which is consistent with an ordered bimolecular transition state. Jencks demonstrated that the reaction of anionic nucleophiles with α-glucopyranosyl fluoride has a linear dependence on concentration of the nucleophile and occurs with inversion of configuration, providing evidence for a concerted bimolecular S_N2 reaction.[7] We interpret our results in a similar manner, and thus at low concentrations, hydroxide reacts with PNPGlc in a concerted, bimolecular reaction as shown in **Fig. 1d**.

Under strongly basic conditions the pH-rate constant plot is independent of hydroxide concentration (slope = 0.022 ± 0.008, k_{NGP} = 0.27 min^{-1}), and product analysis of the hydrolysis reaction in ^{18}O-water, and in a mixture of methanol/water, provides evidence for nucleophilic aromatic substitution (**Fig. 1f**), bimolecular S_N2 substitution at the anomeric position (**Fig. 1d**), and a mechanism involving neighboring group participation that leads to both glucose and 1,6-anhydroglucose (**Fig. 1e**). The major route at pH 12.42 at 90 °C is neighboring group participation. The reaction displayed an inverse solvent isotope effect of $k(HO^-)/k(DO^-)$ = 0.6 ± 0.2. These solvent isotope effects are similar to those reported by Gasman and Johnson for hydrolysis of 4-nitrophenyl β-D-galactoside (PNPGal; $k(HO^-)/k(DO^-)$ = 0.73 ± 0.02) and PNPMan ($k(HO^-)/k(DO^-)$ = 0.70 ± 0.01).[22] This inverse solvent isotope effect indicates that 2-oxyanion attack is the rate limiting step. The apparent enthalpy of activation for PNPGlc ($\Delta H^{\ddagger}$ = 20.8 kcal mol^{-1}) is in reasonable agreement with that reported by Snyder and Link ($\Delta H^{\ddagger}$ = 25.8 kcal mol^{-1}) measured under similar conditions.[22]

Conclusion

In this article we report the pH-rate constant profile for the hydrolysis of PNPGlc, which allowed the identification of four major mechanistic regimes, and detailed kinetic studies allowed identification of the mechanism(s) that operate within these ranges. The

present work highlights the complexity of hydrolytic reactions of aryl 1,2-*trans* glycosides, which aside from the minor S_NAr process are united through the stabilization of developing positive charge at the anomeric centre at the transition state by the endocyclic ring oxygen. The present work provides useful reference data to understand the rate enhancements achieved by enzymes. The most significant rate enhancements occur at the pH extremes, through specific acid or specific base catalyzed reactions. By contrast the enzymatic cleavage catalyzed by glycosidases are general acid and/or base catalyzed. Broadly, glycosidases operate at intermediate pH ranges and utilize general catalysis to assist substitution reactions at the anomeric centre by water or an enzymatic nucleophile.[31] However, a mechanism involving neighboring-group participation by the 2-hydroxyl of an α-mannoside (also likely benefiting from general base catalysis) has been demonstrated for a bacterial endo-α-1,2-mannosidase,[32] which shares obvious similarities to that studied here.

Experimental

General

4-Nitrophenyl β-D-glucopyranoside (PNPGlc) was synthesized as described[33] and recrystallized to purity, as assessed by ^{1}H NMR spectroscopy. NMR spectroscopy was conducted using 400 and 600 MHz instruments. ^{18}O-water (Marshall Isotopes Ltd, 97%) and ^{2}H-water (Sigma Aldrich, 99.9%) were used for mechanism and kinetic studies, respectively. Mass spectrometry was performed using electrospray ionization and an OrbiTrap instrument. pH values of solutions and buffers at elevated temperature were calculated from pH measured at 25 °C using the temperature sensitivity coefficients of the pK_a values of H_2O or of buffers, using ΔpH = ΔpK_a, and d(pK_a)/dT describes the change of the pK_a at an increase of temperature by 1 °C.[34] Water: pK_w = 12.42;[35] phosphate/citric acid, pH range 4-5 pK_a = 7.20, 2.79, respectively, temperature coefficient = –0.0028/0); phosphate, pH range 6-8, pK_2 = 7.20, temperature coefficient = –0.0028, and bicarbonate/carbonate, pH range 9.2-11, pK_{a1} = 6.35, temperature coefficient = –0.0055, pK_{a2} = 10.32, temperature coefficient = –0.009.

Measurement of reaction rates. A Cary3500 UV-Vis spectrophotometry was used to monitor rates of cleavage of PNPGlc by monitoring the released 4-nitrophenol/4-nitrophenolate anion (**Fig. S1**). For continuous assays, reactions were monitored at the isosbestic point of 350 nm using an extinction coefficient (ε), ε_{PNP} = 6.212 mM^{-1} cm^{-1}. For stopped assays, an aliquot was taken from the reaction mixture and alkalinized to pH 10 by

quenching with 2 M Na_2CO_3, then 4-nitrophenolate anion was quantified at 400 nm using ε_{PNP} = 16.14 mM^{-1} cm^{-1} (**Tables S1**, **S2; Fig. S2**). All spectrophotometric measurements were carried out under pseudo-first order conditions with low substrate concentration (1-5 mM) and high concentration of the relevant catalyst (H_3O^+, buffer, or HO^-). Spectroscopic absorbances were measured against a reference cell containing 1 M HCl or NaOH, or 2 M Na_2CO_3.

Reaction rates at varying pH. Individual reactions contained 1-5 mM PNPGlc. For reactions at pH < 4, solutions were prepared by dilution of aq HCl and contained 2 M NaCl. In the range pH 4-11 phosphate and carbonate buffers were used, typically 1 M buffer and 2 M NaCl. In the range of pH 12-14 standardized NaOH was diluted to the final pH and contained 2 M NaCl. Reactions were heated at 75-90 °C for 2-196 h. Reactions at pH 0 and > 11 were performed in semi-micro quartz cuvettes at < 75 °C, and changes in absorbance monitored directly in a UV-Vis spectrophotometer at 350 nm, with rates calculated using the Beer-Lambert law. Very slow reactions suffered from evaporation of solvent, and in these cases, reactions were performed in tightly-sealed Wheaton vials. At various time points aliquots were sampled and added to 2 M Na_2CO_3 and the absorbance of the sample was measured directly at 400 nm. Rates were extrapolated to 90 °C using the Arrhenius parameters determined as outlined below. After correcting for salt, buffer and any other effects data was fit to the modified Henderson-Hasselbach equation.

Salt effects. Reactions were performed by varying concentration of NaCl from 0.25-2 M. The data gave a straight line and extrapolation to [NaCl] = 0 allowed estimation of k_0 and slope of the rate constant. In the acidic or basic regions reactions were monitored by UV/Vis spectroscopy.

In the pH-independent region reactions were conducted in water buffered by 0.005 M phosphate buffer, with concentrations of NaCl varied in the range 0.25–2 M. Sub-samples taken at different time intervals were evaporated to dryness and redissolved in D_2O and studied by ^1H NMR spectroscopy. The rates were determined by monitoring the formation of product (PNP) with time, by plotting the product integration ratio, $f = n_A/(n_A + n_B)$, where n_A is the integration of PNP aromatic proton, n_B is the integration of the PNP-β-Glc aromatic protons. The calculated product ratio was plotted as a function of time using $k = f/t$.

Buffer effects. Rates were extrapolated to zero buffer by holding the pH constant and varying the buffer concentration. At pH values < 1.42, a plot of rate versus [buffer] gave a

straight line with *y*-intercept being the rate at zero buffer and the slope, k_{buffer}, the general catalysed rate constant.

Product analysis. To assess the identity and relative proportions of products, reactions were run to approximately 50% completion, then were evaporated to dryness. For NMR analysis, samples were dissolved in d_6-DMSO or D_2O. For mass spectrometric analysis samples were dissolved in MeOH.

Activation parameters. The Arrhenius equation was used to calculate the thermodynamic parameters of the hydrolysis reaction. The rate of hydrolysis of 1 mM PNPGlc was measured at 350 or 400 nm in solutions of the appropriate pH (**Table 2**) at 75–45 °C and 150 mM NaCl at four different temperatures. Plotting the natural logarithm of k_{obs} as a function of the inverse of the temperatures gives a straight line with slope of $\frac{-E_a}{R}$ and a *y* intercept of ln A, and allowed calculation of the activation energy, E_a, and the pre-exponential factor in the Arrhenius relationship, ln A (eq. 3):

$$\ln A = \ln k + E_a / R T_1 \qquad \text{eq. 3}$$

The activation parameters allowed calculation of the enthalpy and entropy of activation at 298.1 K, according to equations 4 and 5 derived from transition state theory:

$$\Delta H^{\ddagger} = E_a - RT \qquad \text{eq. 4}$$

$$\Delta S^{\ddagger} = R\left(\ln A - \ln \frac{K_B T}{h}\right) R \qquad \text{eq. 5}$$

where K_B is Boltzmann constant, *h* is Planck's constant, T is the temperature, and R is the ideal gas constant.

Solvent isotope effects. The solvent isotope effect in the acidic region was measured in solutions contained $[H_3O^+]$ = 1 M or $[D_3O^+]$ = 1 M (prepared by 1:10 dilution of 10 M HCl into H_2O or D_2O) and [NaCl] = 150 mM, with [PNPGlc] = 0.1 mM at 75 °C. Initial rates were measured using a continuous assay at 350 nm in triplicate to either calculate standard deviation (SD) or standard error (SR).

The solvent isotope effect in the pH independent region was measured in H_2O or D_2O pH = pD = 6.8 (determined using the correction for a glass electrode of pD = pH + 0.41),

with [phosphate] = 0.005 M, [NaCl] = 150 mM, and [PNPGlc] = 1 mM at 90 °C or with [phosphate] = 1 M, [NaCl] = 2 M. Initial rates were measured in triplicate using a stopped assay after quenching with base.

The solvent isotope effect was measured in H_2O or D_2O solvent at pH = pD = 13.26, with [NaOD] = [NaOH] = 1 M (prepared by 1:10 dilution of 10 M NaOH into H_2O or D_2O) and [NaCl] = 150 mM, and [PNPGlc] = 0.1 mM at 75 °C. Initial rates were measured in triplicate using a continuous assay at 400 nm.

The proton inventory experiment was conducted in the pH-independent region using phosphate buffer made from a mixed solution of D_2O and H_2O, p(H,D) = 5.8 at 90 °C. According to guidance from Rubinson[36] no corrections are needed in mixed H_2O-D_2O buffers for p(H,D) measurements < 8. The preparation of buffer was carried out using stock solutions of the 1 M acidic and basic buffer components in D_2O, each of which contains 2 M NaCl, and another two stock solutions made in the same manner in H_2O. Each set of stock solutions were combined to make 1 M buffers of pD 5.8 and pH 5.8 (determined using the correction for a glass electrode of pD = pH + 0.41) and ionic strength 2 M NaCl. Reaction solutions of a total volume of 1 ml were obtained by mixing the appropriate amount of D_2O and H_2O buffers to give samples with varying content of D_2O (0, 20, 50, 80 and 100%) where the 0 and 100% samples were made using the unmixed D_2O and H_2O buffers. Rate data was analysed using the linear Gross-Butler equation (eq 6):

$$\frac{k_n}{k_0} = \frac{(1-n+\varphi_1^{TS})}{(1-n+\varphi_1^{GS})} \frac{k_n}{k_0} = \frac{(1-n+n\varphi_1^{TS})}{(1-n+n\varphi_1^{GS})}$$

eq. 6

where k_n k_n = the rate constant at atom fractionation deuterium n, k_0 = the rate constant in pure water, and φ_1^{TS} and $\varphi_1^{TS} and \varphi_1^{GS}$ φ_1^{GS} are the fractionation factors of the exchangeable proton in the transition and ground state.

Calculation of predicted solvent isotope effects. The solvent isotope effect was calculated using the isotopic fractionation factor φ.[27] The isotopic fractionation factor is the preference of a hydrogen to be at any site in the solute over the solvent. Thus, in the equilibrium reaction where the substrate is converted to its conjugate acid the equilibrium fractionation factors

defined by equation 7 allows the calculation of the preferred hydron site as an equilibrium ratio.

$$\frac{K_H}{K_D} = \frac{[RD]/[RH]}{[ROH]/[ROD]} / \frac{[PD]/[PH]}{[POD]/[POH]} = ¿ \frac{\varphi_R}{\varphi_P} ¿ \qquad \text{eq. 7}$$

Associated Content

Supporting information

Electronic supplementary information (ESI) available. See DOI:

Kinetic measurements including rates of hydrolysis under various pH and buffer conditions, dependencies of rates upon temperature, solvent isotope effects and proton inventory. NMR spectra for sample reactions, **Tables S1-14** and **Figures S1-14** (PDF).

Author Information

Corresponding Author

Spencer J. Williams, Email: sjwill@unimelb.edu.au

Notes

The authors declare no competing financial interest.

Acknowledgements

This work was supported by a grant from the Australian Research Council (DP180101957, DP210100233). AA thanks Jazan University for financial support and thanks the Saudi Arabian Cultural Mission (SACM).

References

1. Colombo, C.; Bennet, A. J., The physical organic chemistry of glycopyranosyl transfer reactions in solution and enzyme-catalyzed. *Curr. Opin. Chem. Biol.* **2019,** *53*, 145-157.

2. Amyes, T. L.; Jencks, W. P., Lifetimes of oxocarbenium ions in aqueous solution from common ion inhibition of the solvolysis of α-azido ethers by added azide ion. *J. Am. Chem. Soc.* **1989,** *111*, 7888-7900.

3. Zhu, J.; Bennet, A. J., Hydrolysis of (2-Deoxy-α-D-Glucopyranosyl)pyridinium Salts: The 2-Deoxyglucosyl Oxocarbenium Is Not Solvent-Equilibrated in Water. *J. Am. Chem. Soc.* **1998,** *120*, 3887-3893.

4. Indurugalla, D.; Bennet, A. J., A Kinetic Isotope Effect Study on the Hydrolysis Reactions of Methyl Xylopyranosides and Methyl 5-Thioxylopyranosides: Oxygen versus Sulfur Stabilization of Carbenium Ions. *J. Am. Chem. Soc.* **2001,** *123*, 10889-10898.

5. Sinnott, M. L.; Jencks, W. P., Solvolysis of D-glucopyranosyl derivatives in mixtures of ethanol and 2,2,2-trifluoroethanol. *J. Am. Chem. Soc.* **1980,** *102*, 2026-2032.

6. Banait, N. S.; Jencks, W. P., Reactions of anionic nucleophiles with α-D-glucopyranosyl fluoride in aqueous solution through a concerted, A_ND_N (S_N2) mechanism. *J. Am. Chem. Soc.* **1991,** *113*, 7951-7958.

7. Banait, N. S.; Jencks, W. P., General-acid and general-base catalysis of the cleavage of a-D-glucopyranosyl fluoride. *J. Am. Chem. Soc.* **1991,** *113*, 7958-7963.

8. Huang, X.; Surry, C.; Hiebert, T.; Bennet, A. J., Hydrolysis of (2-Deoxy-β-D-glucopyranosyl)pyridinium Salts. *J. Am. Chem. Soc.* **1995,** *117*, 10614-10621.

9. BeMiller, J. N., Acid-catalyzed hydrolysis of glycosides. *Adv. Carbohydr. Chem.* **1967,** *22*, 25-108.

10. Bunton, C. A.; Lewis, T. A.; Llewellyn, D. R.; Vernon, C. A., Mechanisms of reactions in the sugar series. Part I. The acid-catalysed hydrolysis of α- and β-methyl and α- and β-phenyl D-glucopyranosides. *J. Chem. Soc.* **1955**, 4419-4423.

11. Rosenberg, S.; Kirsch, J. F., Oxygen-18 leaving group kinetic isotope effects on the hydrolysis of nitrophenyl glycosides. 2. Lysozyme and β-glucosidase: acid and alkaline hydrolysis. *Biochemistry* **1981,** *20*, 3196-3204.

12. Overend, W. G.; Rees, C. W.; Sequeira, J. S., 675. Reactions at position 1 of carbohydrates. Part III. The acid-catalysed hydrolysis of glycosides. *J. Chem. Soc.* **1962**, 3429-3440.

13. Nath, R. L.; Rydon, H. N., The influence of structure on the hydrolysis of substituted phenyl β-d-glucosides by emulsin. *Biochem. J.* **1954,** *57*, 1-10.

14. Hall, A. N.; Hollingshead, S.; Rydon, H. N., The acid and alkaline hydrolysis of some substituted phenyl alpha-D-glucosides. *J. Chem. Soc.* **1961**, 4290-4295.

15. Wolfenden, R.; Lu, X.; Young, G., Spontaneous hydrolysis of glycosides. *J. Am. Chem. Soc.* **1998,** *120*, 6814-6815.

16. Namchuk, M. N.; McCarter, J. D.; Becalski, A.; Andrews, T.; Withers, S. G., The Role of Sugar Substituents in Glycoside Hydrolysis. *J. Am. Chem. Soc.* **2000,** *122*, 1270-1277.

17. Ballou, C. E., Alkali-Sensitive Glycosides. *Adv. Carbohydr. Chem.* **1954,** *9*, 59-95.

18. Snyder, J. A.; Link, K. P., Acid and Alkaline Hydrolysis Rates and Heats of Activation of Some o- and p-Nitrophenyl Glycosides1. *J. Am. Chem. Soc.* **1952,** *74*, 1883-1884.

19. Dyfverman, A.; Lindberg, B., The Alkaline Hydrolysis of Phenyl β-Glucosides. A Kinetic Investigation. *Acta Chem. Scand.* **1950**, 878-884.

20. Koehler, L. H.; Hudson, C. S., Some Reactions of the 2,4,6-Tribromophenyl β-D-Pyranosides of Glucose and Xylose. *J. Am. Chem. Soc.* **1950,** *72*, 981-983.

21. McCloskey, C. M.; Coleman, G. H., A proposed inversion mechanism for the formation of levoglucosan from phenyl β-D-glucoside and trimethylglucosylammonium compounds. *J. Org. Chem.* **1945,** *10*, 184-193.

22. Gasman, R. C.; Johnson, D. C., C-2 Oxyanion Participation in the Base-Catalyzed Cleavage of p-Nitrophenyl β-D-Galactopyranoside and p-Nitrophenyl α-D-Mannopyranoside. *J. Org. Chem.* **1966,** *31*, 1830-1838.

23. Speciale, G.; Farren-Dai, M.; Shidmoossavee, F. S.; Williams, S. J.; Bennet, A. J., C2-Oxyanion neighboring group participation: Transition state structure for the hydroxide-promoted hydrolysis of 4-nitrophenyl α-D-mannopyranoside. *J. Am. Chem. Soc.* **2016,** *138*, 14012-14019.

24. Chan, J.; Sannikova, N.; Tang, A.; Bennet, A. J., Transition-State Structure for the

Quintessential S_N2 Reaction of a Carbohydrate: Reaction of α-Glucopyranosyl Fluoride with Azide Ion in Water. *J. Am. Chem. Soc.* **2014,** *136*, 12225-12228.

25. Alibrandi, G.; Coppolino, S.; Micali, N.; Villari, A., Variable pH kinetics: An easy determination of pH–rate profile. *J. Pharm. Sci.* **2001,** *90*, 270-274.

26. Loudon, G. M., Mechanistic interpretation of pH-rate profiles. *J. Chem. Educ.* **1991,** *68*, 973.

27. Schowen, R. L., Mechanistic deductions from solvent isotope effects. *Progress Phys. Org. Chem.* **1972,** *9*, 275-332.

28. Dean, J. A., *Lange's Handbook of Chemistry*. McGraw-Hill Inc: New York, 1999.

29. Venkatasubban, K. S.; Schowen, R. L., The proton inventory technique. *CRC Crit. Rev. Biochem.* **1984,** *17*, 1-44.

30. Bennet, A. J.; Sinnott, M. L., Complete kinetic isotope effect description of transition states for acid-catalyzed hydrolyses of methyl α- and β-glucopyranosides. *J. Am. Chem. Soc.* **1986,** *108*, 7287-7294.

31. Zechel, D. L.; Withers, S. G., Glycosidase mechanisms: Anatomy of a finely tuned catalyst. *Acc. Chem. Res.* **2000,** *33*, 11-18.

32. Sobala, L. F.; Speciale, G.; Zhu, S.; Raich, L. s.; Sannikova, N.; Thompson, A. J.; Hakki, Z.; Lu, D.; Shamsi Kazem Abadi, S.; Lewis, A. R.; Rojas-Cervellera, V.; Bernardo-Seisdedos, G.; Zhang, Y.; Millet, O.; Jiménez-Barbero, J.; Bennet, A. J.; Sollogoub, M.; Rovira, C.; Davies, G. J.; Williams, S. J., An Epoxide Intermediate in Glycosidase Catalysis. *ACS Cent. Sci.* **2020,** *6*, 760-770.

33. Dess, D.; Kleine, H. P.; Weinberg, D. V.; Kaufman, R. J.; Sidhu, R. S., Phase-Transfer Catalyzed Synthesis of Acetylated Aryl β-D-Glucopyranosides and Aryl β-D-Galactopyranosides. *Synthesis* **1981,** *1981*, 883-885.

34. Ellis, K. J.; Morrison, J. F., Buffers of constant ionic strength for studying pH-dependent processes. In *Methods Enzymol.*, Purich, D. L., Ed. Academic Press: 1982; Vol. 87, pp 405-426.

35. Bandura, A. V.; Lvov, S. N., The Ionization Constant of Water over Wide Ranges of Temperature and Density. *J. Phys. Chem. Ref. Data* **2005,** *35*, 15-30.

36. Rubinson, K. A., Practical corrections for p(H,D) measurements in mixed H_2O/D_2O biological buffers. *Anal. Methods* **2017,** *9*, 2744-2750.

Table of Contents Entry

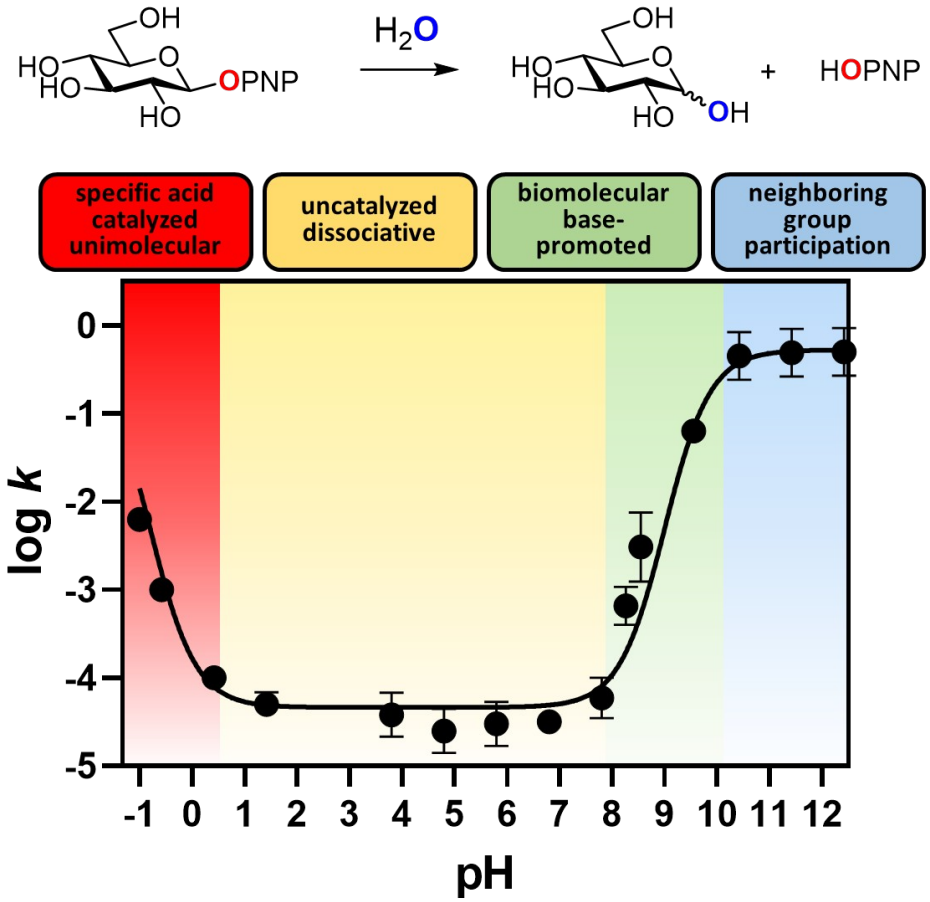

SUPPLEMENTARY INFORMATION

Unimolecular, bimolecular and intramolecular hydrolysis mechanisms of 4-nitrophenyl β-D-glucopyranoside

Amani Alhifthi and Spencer J. Williams*

School of Chemistry and Bio21 Molecular Science and Biotechnology Institute, University of Melbourne, Parkville 3010, Victoria, Australia

Table of Contents

Table S1. Calibration data for absorbance of 4-nitrophenolate ($PNPO^-$) as a percentage of a mixture of $PNPO^-$ and 4-nitrophenyl β-D-glucopyranoside (PNPGlc) in [NaOH] = 1 M solution.

This data was used to generate a calibration curve (**Figure S2a**) in which [$PNPO^-$] is plotted versus absorbance at 400 nm.

% $PNPO^-$	[$PNPO^-$] mM	Abs 400 nm
0	0	0.0117
5	0.005	0.0891
10	0.01	0.1591
15	0.015	0.1582
20	0.02	0.3176
25	0.025	0.4487
30	0.03	0.4698
35	0.035	0.5298
40	0.04	0.5826
45	0.045	0.7071
50	0.05	0.8437
55	0.055	0.8954
60	0.06	0.9922
65	0.065	1.0585
70	0.07	1.2207
75	0.075	1.2262
80	0.08	1.226
85	0.085	1.3738
90	0.09	1.4369
95	0.095	1.4998
100	0.1	1.5886

Table S2. Calibration data for absorbance at 350 nm of solutions of $PNPO^-$/PNPOH or PNPGlc in neutral solution (pH = 7).

This data was used to generate calibration curves (**Figure S2b** and **c**) in which [$PNPO^-$/PNPOH] or [PNPGlc] was plotted versus absorbance at 350 nm.

[$PNPO^-$/PNPOH] or [PNPGlc] (mM)	**Absorbance (350 nm)**	
0.1	0.625	0.144
0.075	0.43	0.1
0.05	0.314	0.069
0.025	0.146	0.033
0.012	-	0.014

Table S3. Rates of hydrolysis of PNPGlc under acidic conditions ([HCl] = 0.26 M, 55 °C) with varying salt concentrations.

Slope (v, min^{-1}) values from **Figure S3a**. The rate constants from this table are plotted versus [salt] in **Figure S4a**.

[NaCl], M	**slope (v, min^{-1})** [b]	***k* = *v* / [S] Δε350 min^{-1} (y x 10^4)** [c]	**y` (x 10^5)** [d]	**r^2**
2	0.00018	3.8	1	0.99
1	0.00013	2.8	3	0.99
0.5	0.00009	2.0	4	0.99
0.25	0.00008	1.8	4	0.99
0 [a]	-	1.58	0.86	-

[a] k_0 is the rate extrapolated to zero salt. [b] v (min^{-1}) obtained from absorbance-time plots at 350 nm, continuous assays. [c] Substrate concentration [S] = 0.1 mM. Δε350 = 4.46 nM^{-1} cm^{-1}. [d] Standard error = y`.

Table S4. Rates of hydrolysis of PNPGlc in the pH-independent region at 90 °C with 0.005 M phosphate buffer (pH 6.8 at 90 °C) in the presence of three different salts.

Slope values from **Figure S3e-f**. The rate constants of this table are plotted versus [salt] in **Figure S4b**.

[salt] (M)	NaCl	KCl	$NaClO_4$
	slope (v) = k min^{-1} (y x 10^5)[a]		
2	2.847	2.083	1.453
1	2.138	2.155	1.4
0.5	1.928	2.029	1.4
0.25	2.078	-	1.509
k_0	1.74±0.07	2.02±0.03	1.5±0.03

[a] Slope (v) = k min^{-1} obtained by plotting (f) vs time (mins), $k = f/t$ and $f = (n_a/(n_a+n_b)$, where n_a is the integration of 4-nitrophenol/phenolate aromatic protons, and n_b is the integration of the PNPGlc aromatic proton signals a and b. Chemical shifts: ^{1}H NMR (400 MHz, D_2O), δ a = 8.25, 7.05 ppm and δ b = 8.33, 7.31 ppm.

Table S5. Rates of hydrolysis of PNPGlc in the strongly basic region ([NaOH] = 1 M, 55 °C) under varying salt concentration.

k values from **Figure S3c**. The rate constants of this table are plotted versus [salt] in **Figure S4c**.

[NaCl], M	*k* min^{-1} (y x 10^3) [a]	y' (x 10^3) [b]	Δy [b]	r^2
1.58	35	2	0.06	0.99
1	41	6	0.15	0.99
0.5	36	1	0.03	0.99
0.25	46	7	0.15	0.99
0.1	40	1	0.025	0.99
0.07	49	3	0.06	0.99
0.04	40	7	0.18	0.99
0.02	49	2	0.040	0.99
0	39	2	0.051	0.99

[a] *k* (v, min^{-1}) obtained from absorbance-time plots using a one-phase decay; 400 nm, continuous assays. [b] Relative error = Δy = (y`/y), (y`= standard error).

Table S6. Buffer effect for the hydrolysis of PNPGlc in the pH-independent-region (90 °C).

Slope values from **Figure S5a-c**. The rate constants from this table are plotted versus [buffer] in **Figure S5d**.

[buffer] M	pH 3.8		pH 4.8 and pH 5.8		
	k **min^{-1} (y x 10^5)**	**Δy** [a]	**Slope (*v*) = *k*** **min^{-1} (y x 10^5)**	**Δy** [a]	**S** **n**
1	8.98	0.032	9.60	0.031	
0.75	7.56	0.028	-	-	
0.5	6.40	0.033	6.00	0.012	
0.25	5.12	0.046	4.20	0.027	
k_o [b]	3.83	0.024	2.40	0.019	
k_{buffer} (M^{-1} min^{-1})	5.10	0.027	7.20	0.046	

[a] Relative error = Δy = (y`/y), standard error = y`. [b] Extrapolated rate to zero buffer. Slope (v, min^{-1}) measured at 400 nM, stopped assays.

Table S7. Buffer effect for the hydrolysis of PNPGlc in the weakly basic region (90 °C).

Slope values from **Figure S6a-c**. The rate constants from this table are plotted versus [buffer] in **Figure S6d**.

[buffer] M	pH 7.8		pH 8.26		
	k **min^{-1} (y x 10^5)**	**Δy** [a]	**Slope (*v*) = *k*** **min^{-1} (y x 10^4)**	**Δy** [a]	**n**
1	6.08	0.06	6.37	1	
0.5	5.8	0.06	6.03	0.5	
0.25	6.4	0.06	6.16	0.25	
k_o [b]	6.25	0.085	6	k_o [b]	
k_{buffer} (M^{-1} min^{-1})	-0.3	3	0.34	0.9	

[a] Relative error = Δy = (y`/y), standard error = y`. [b] Extrapolated rate to zero buffer. Slope (v, min^{-1}) measured at 400 nM, stopped assays.

Table S8. Rates of hydrolysis of PNPGlc versus temperature in the acidic region (pH 0.58, 0.1 mM PNPGlc, 2 M NaCl).

The rate constants of this table are obtained from the slope values in **Figure S8a**.

T (K)	Slope (*v*, min^{-1})	$k = v / [S]$ $\Delta\varepsilon 350$ min^{-1}	$k = v \times 0.42$ min^{-1} (y x 10^3) [a]	Δy [b]	(1/T x 10^4), K^{-1}	log *k*
363.15 [c]	-	-	6.20		27.5	-2.21
348.15	0.00224	0.00503	2.10	0.004	28.72	-2.68
338.15	0.00117	0.00263	1.09	0.003	29.57	-2.96
328.15	0.00036	0.00080	0.34	0.012	30.47	-3.47
318.15	0.00008	0.00017	0.07	0.025	31.43	-4.15

[a] Salt effect correction factor = 0.42, from data in Table S3. [b] Relative error = Δy = (y`/y), standard error = y`. Substrate concentration, [S] = 0.1 mM. Δε350 = 4.46 nM^{-1} cm^{-1}. [c] Extrapolated rate constant at 90 °C using ln k = ln A – E_a/RT, where ln A = 29.82, E_a = 105443.311 J/mol, R = 8.314 J/(mol K), T = 363.15 K.

Table S9. Rates of hydrolysis of PNPGlc versus temperature in the pH-independent region (pH 5.8).

The rate constants of this table are obtained from the slope values in **Figure S8b**.

T (K)	Slope (*v* x10^5, min^{-1})	$k = v \times 0.25$ k min^{-1} (y x10^5) [a]	Δy [b]	1/T (x 10^4), K^{-1}	log *k*
363.15	9.6	2.4	0.1	27.53	-4.61
348.15	1.6	0.4	0.2	28.72	-5.39
338.15	0.45	0.1	0.1	29.57	-5.95

[a] Buffer effect correction factor = 0.25 from data in Table S6. [b] Relative error = Δy = (y`/y), standard error = y`.

Table S10. Rates of hydrolysis of PNPGlc versus temperature in the weakly basic region (pH 8.55).

The rate constants of this table are obtained from **Figure S8c**.

T (K)	Slope (*v*) = *k* min^{-1} (y x10^4)	Δy [a]	1/T (x 10^4), K^{-1}	log *k*
338.15	9.00	0.1	29.57	-3.04
348.15	3.00	0.2	28.72	-3.52
363.15	1.00	0.1	27.54	-4.0

[a] Relative error = Δy = (y`/y), standard error = y`.

Table S11. Rates of hydrolysis of PNPGlc versus temperature in the strongly basic region (pH 12.42).

The rate constants of this table are obtained from the slope values in **Figure S8d**.

T (K)	Slope (*v*, min^{-1})	*k* = *v* x 0.89 min^{-1} (y x10^1) [a]	Δy [b]	1/T (x 10^4), K^{-1}	log *k*
318.15	0.0087	0.07	0.13	31.43	-2.15
328.15	0.039	0.34	0.10	30.50	-1.50
338.15	0.098	0.87	0.13	29.60	-1.08
348.15	0.144	1	0.10	28.72	-1
363.15 [c]	-	5	0.13	27.53	-0.3

[a] Correction factor = 0.89 (1 – contribution of bimolecular process – contribution of nucleophilic aromatic substitution = 1 – 0.1 – 0.01). [b] Relative error = Δy = (y`/y), standard error = y`. [c] Extrapolated rate constant at 90 °C using ln k = ln A – E_a/RT, where ln A = 29.82, E_a = 105443.311 J/ mol, R = 8.314 J/(mol K), T = 363.15 K.

Table S12. Solvent isotope effects for the hydrolysis of PNPGlc.

The rate constants of this table are obtained from the slope values in **Figure S9a-e**.

Region (temp)	conditions	slope (v, min^{-1})	k min^{-1} ($y \times 10^5$)	(y') × 10^6 [a]	Δy [a]	r^2
acidic	pD –0.75	0.00146	320 [b]	90	0.006	0.99
(75 °C)	pH –0.75	0.00095	202 [b]	96	0.010	0.99
	k_H/k_D		0.65±0.01	-	-	-
pH independent	pD 6.8	0.0000302	3.02	1.72	0.06	0.99
[buffer] = 0.005 M	pH 6.8	0.0000340	3.40	2.46	0.07	0.98
(90 °C)	k_{H2O}/k_{D2O}		1.1 ± 0.1	-	-	-
pH independent	pD 6.8	0.0000361	3.61	3.39	0.09	0.99
[buffer] = 1 M	pH 6.8	0.000050	5.50	3.36	0.06	0.97
(90 °C)	k_H/k_D		1.52 ± 0.09	-	-	-
mildly basic	pD 8.4	0.0017	177	28.2	0.015	0.99
(90 °C)	pH 8.4	0.00090	90.1	26.02	0.028	0.98
	k_H/k_D		0.50 ± 0.1	-	-	-
strongly basic	pD 13.1	0.065	6570	173.4	0.026	0.99
(55 °C)	pH 13.1	0.031	3150	211.3	0.067	0.98
	k_H/k_D		0.5 ± 0.07	-	-	-

[a] Relative error = Δy = (y`/y), standard error = y`. [b] k = v / [S] Δε350, substrate concentration, [S] = 0.1 mM. Δε350 = 4.46 nM^{-1} cm^{-1}, no salt effect correction, [NaCl] = 150 mM.

Table S13. Calculation of solvent isotope effect (φ^R/φ^P) using the fractionation factors (φ) of reactants (*R*) and products (*P*) for different mechanisms of hydrolysis.

Mechanism	$\frac{R}{P}$	$\frac{\varphi^R}{\varphi^P}$	
Specific acid catalysis $\frac{K_H}{K_D}=\frac{[H_3O$	$\frac{[H_3O]^3}{[ROH]^1[H_2O]^2}$	$\frac{[0.69]^3}{[0.69]^1[1]^1}$	0.476
	$\frac{[OH]^1[ROH]^1}{[POH]^1}$	$\frac{[0.47]^1[1]^1}{[1.23]^1}$	0.43
Bimolecular reaction			
Intermolecular reaction	$\frac{[R—O]^1}{[ROR]^1}$	$\frac{[0.56]^1}{[1]^1}$	0.56

Table S14. Proton inventory for the hydrolysis of PNPGlc in the pH-independent region (p(H,D) 5.8 at 90 ºC).

The rate constants of this table are obtained from the slope values in **Figure S10a**.

n	**Slope (*v*, min^{-1})** [b]	***k* (× 10^5 min^{-1})**	**Avg. SD (× 10^7)**	**No. of trials**
0	0.00007225	7.15	2.5	4
0.2	0.0000675	6.6	5	4
0.5 [a]	0.000059	5.91	4.5	4
0.8	0.0000515	5.2	5	4
1	0.000049	4.8	5	4

[a] $k_{0.5}$ precision = 1.01 %. [b] Slope (v, min^{-1}) measured at 400 nm, stopped assays.

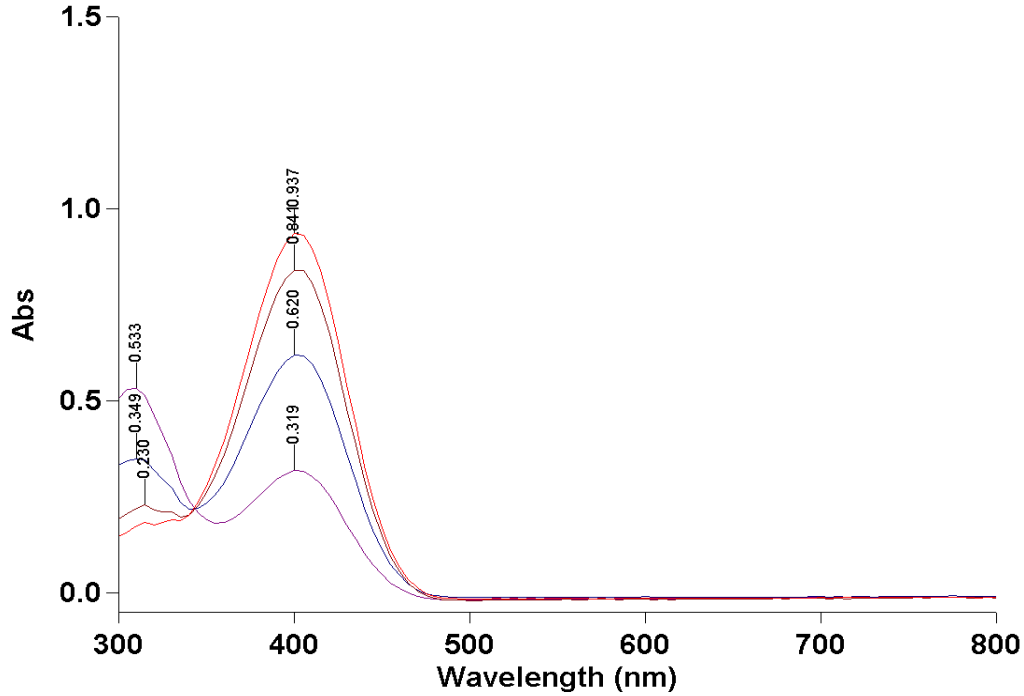

Figure S1. Representative UV-Vis spectra of a mixture of PNPGlc, PNPOH and $PNPO^-$ of four aliquots sampled at 80, 155, 230, or 305 hours from the hydrolysis of PNPGlc at 90 °C in pH 7. $PNPO^-$ has maximum absorbance at 400 nm and the isosbestic point is 350 nm.

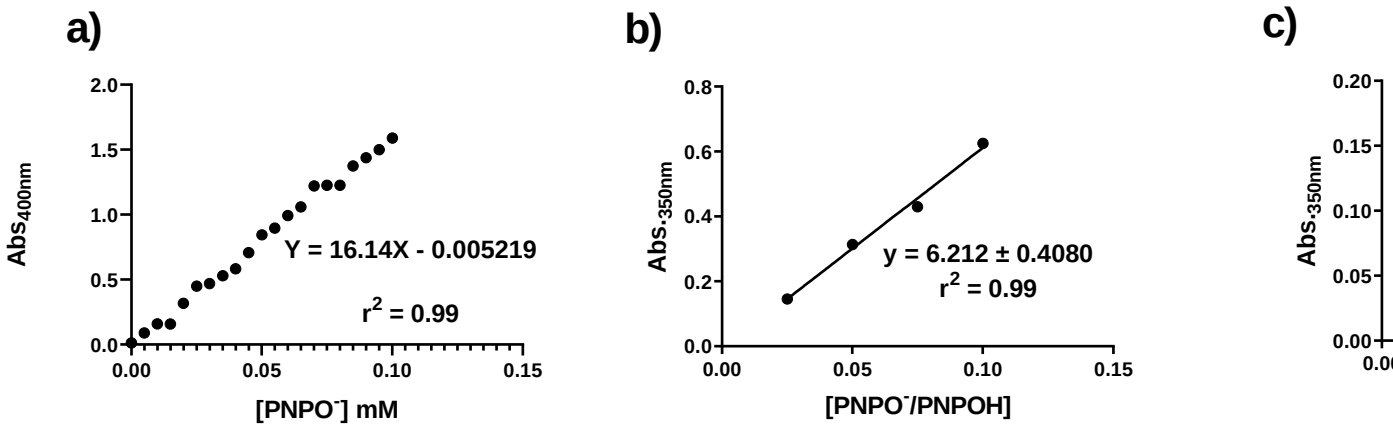

Figure S2. Calibration curves showing relationship of $[PNPO^-]$, $[PNPO^-/PNPOH]$ or [PNPGlc] and absorbance.

a) Absorbance-concentration curve of $[PNPO^-]$ in basic solution [NaOH] = 1 M at 400 nm. **b)** Absorbance-concentration curve of $[PNPO^-/PNPOH]$ in neutral solution (pH = 7) at 350 nm. **c)** Absorbance-concentration curve of [PNPGlc] in neutral solution (pH = 7) at 350 nm.

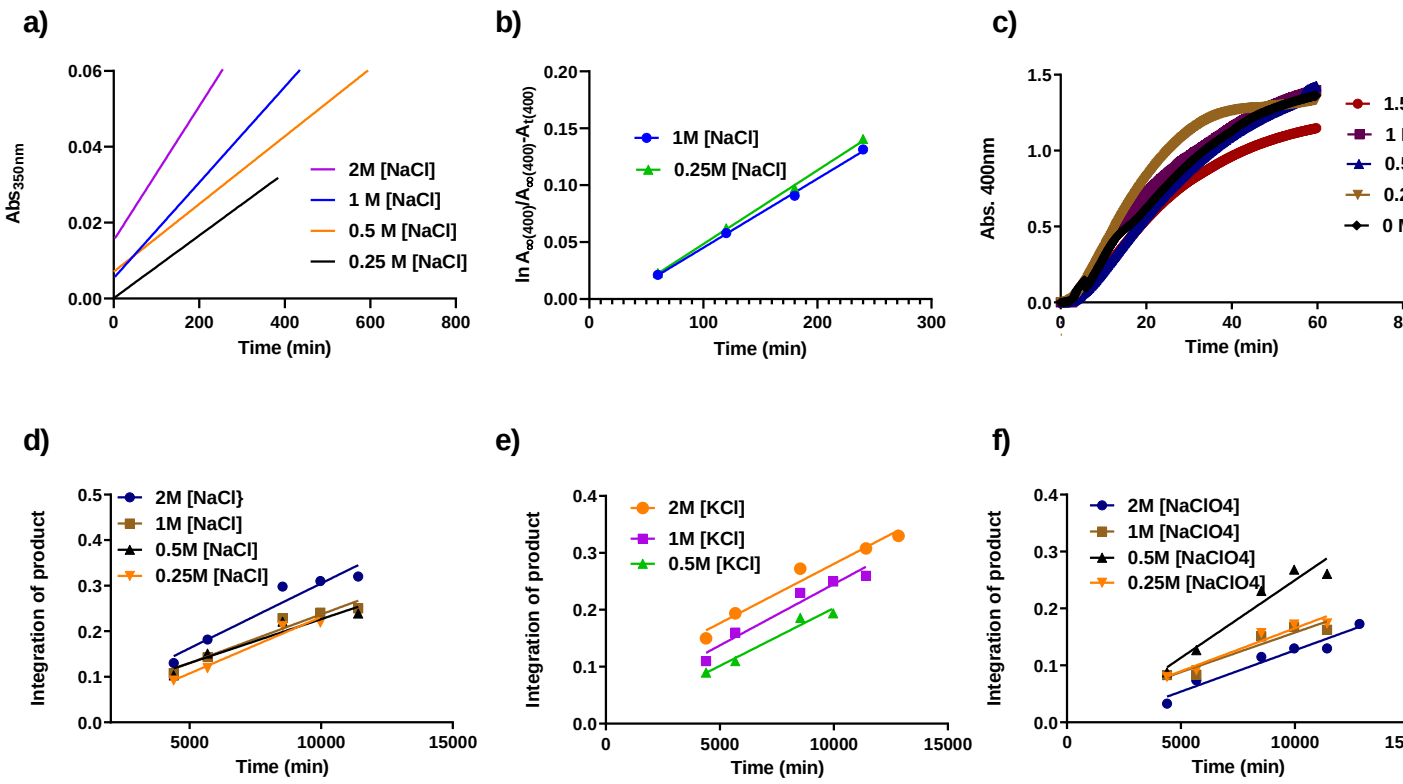

Figure S3. Plots showing formation of product versus time for salt effect upon the hydrolysis of PNPGlc in acidic, pH-independent and basic regions.

a) Absorbance-time curves for salt effect in the acidic region in [HCl] = 0.26 M at 55 °C. **b)** Absorbance-time curves for salt effect in the weakly basic region in pH 8.4 at 90 °C. **c)** Absorbance-time curves for salt effect in the strongly basic region in [NaOH] = 1 M at 55 °C. **d-f)** Product ratio integration-time curves (^{1}H NMR) for salt effect in the pH-independent region for [buffer] = 0.005 M, pH 6.8 at 90 °C in the presence of three different salts (NaCl, KCl, or $NaClO_4$).

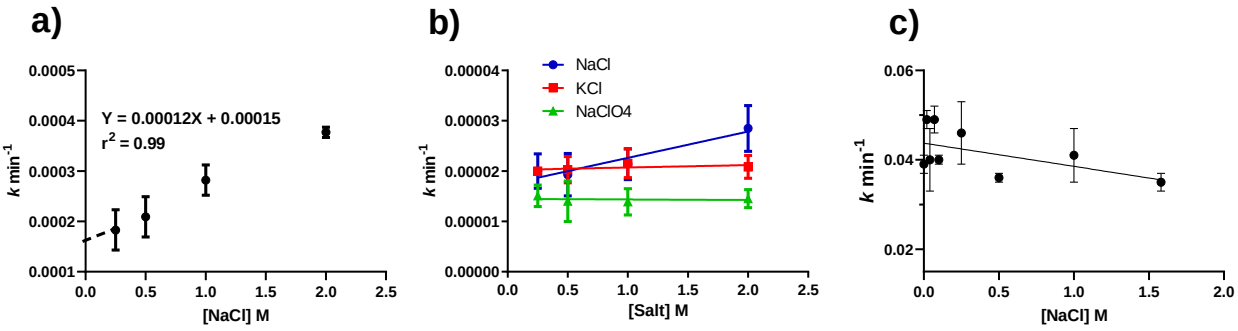

Figure S4. Plots showing the dependencies of the hydrolysis rate constants of PNPGlc on the concentration of salt in the acidic region, pH-independent region, and strongly basic region.

a) Salt effect and rate constant extrapolation to zero salt in the acidic region ([HCl] = 0.26 M at 55 °C). **b)** Salt effect in the pH-independent region ([buffer] = 0.005 M, pH 6.8 at 90 °C). **c)** Salt effect in the strongly basic region ([NaOH] = 1 M at 55 °C).

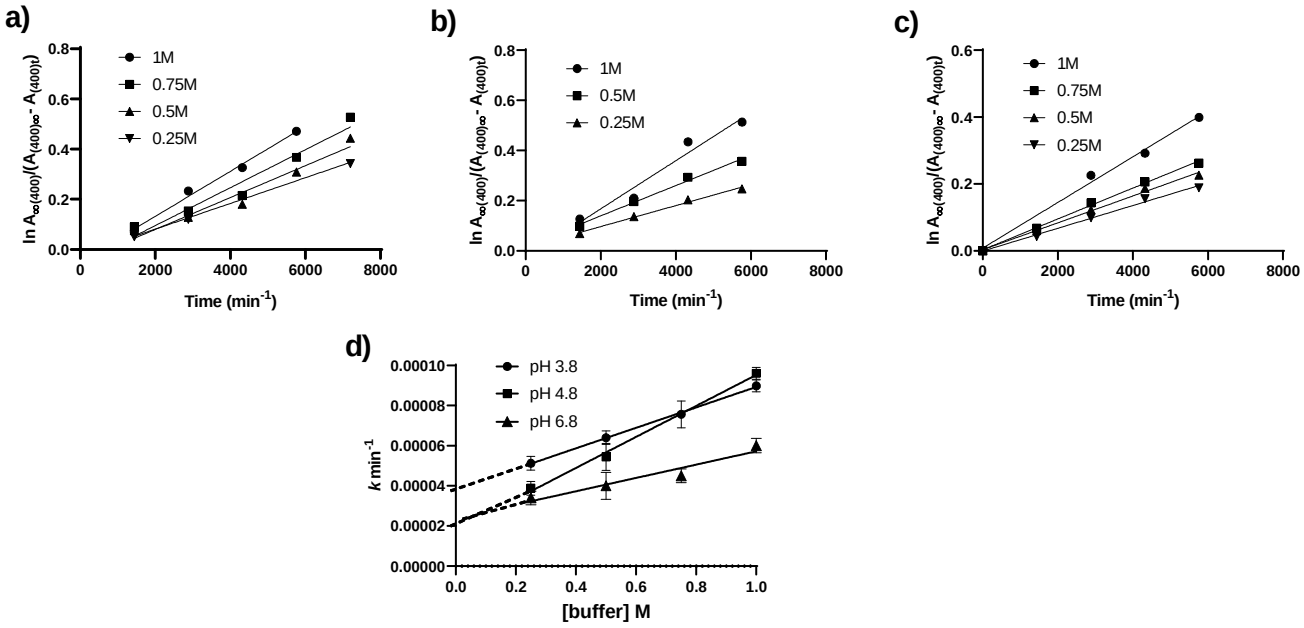

Figure S5. Plots showing formation of product versus time for buffer effect upon the hydrolysis of PNPGlc and the dependencies of the hydrolysis rate constants of PNPGlc on [buffer] in the pH-independent region at 90 °C.

a) Absorption-time curve for buffer effect in pH 3.8. **b)** Absorption-time curve for buffer effect in pH 4.8. **c)** Absorption-time curve for buffer effect in pH 6.8. **d)** Extrapolation to zero buffer concentration across the pH-independent region versus buffer concentration (pH, 3.8, 4.8 and 6.8).

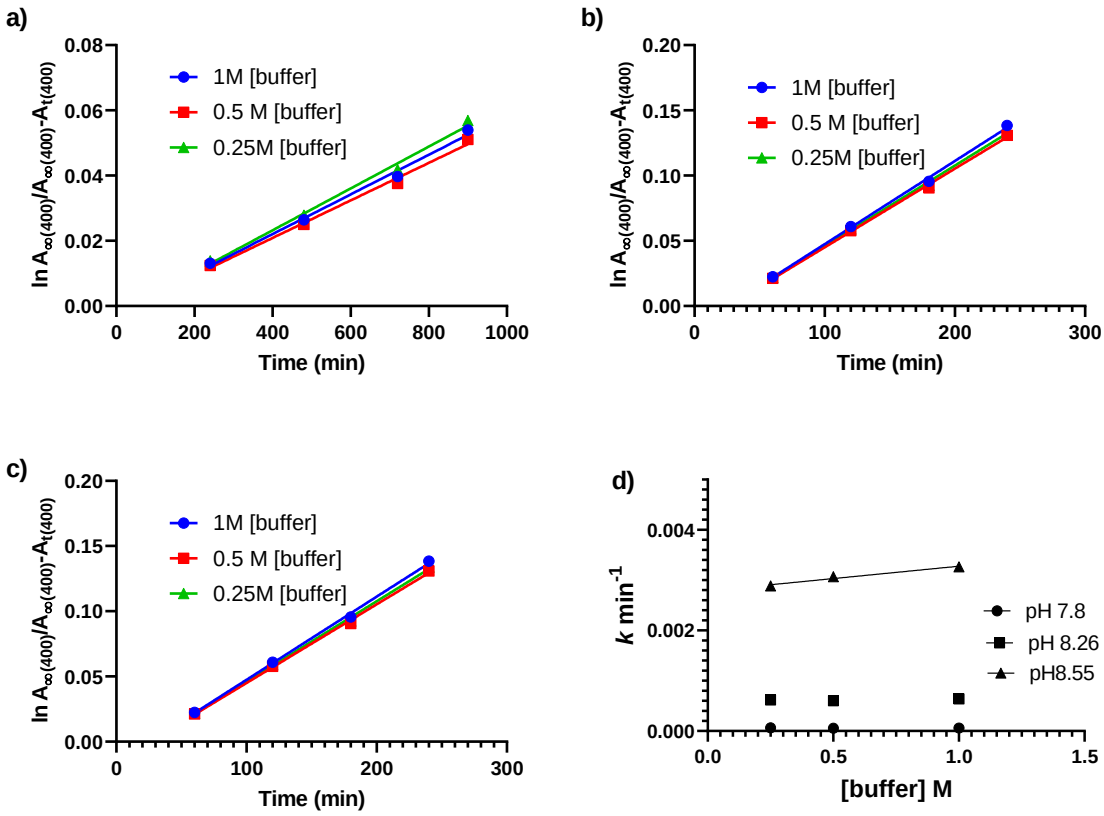

Figure S6. Plots showing formation of product versus time for buffer effect upon the hydrolysis of PNPGlc and the dependencies of the hydrolysis rate constants of PNPGlc on [buffer] in the weakly basic region at 90 °C.

a) Absorption-time curve for buffer effect in pH 7.8. **b)** Absorption-time curve for buffer effect in pH 8.26. **c)** Absorption-time curve for buffer effect in pH 8.55. **d)** Extrapolation to zero buffer concentration across the pH-independent region versus buffer concentration (pH, 7.8, 8.26 and 8.55).

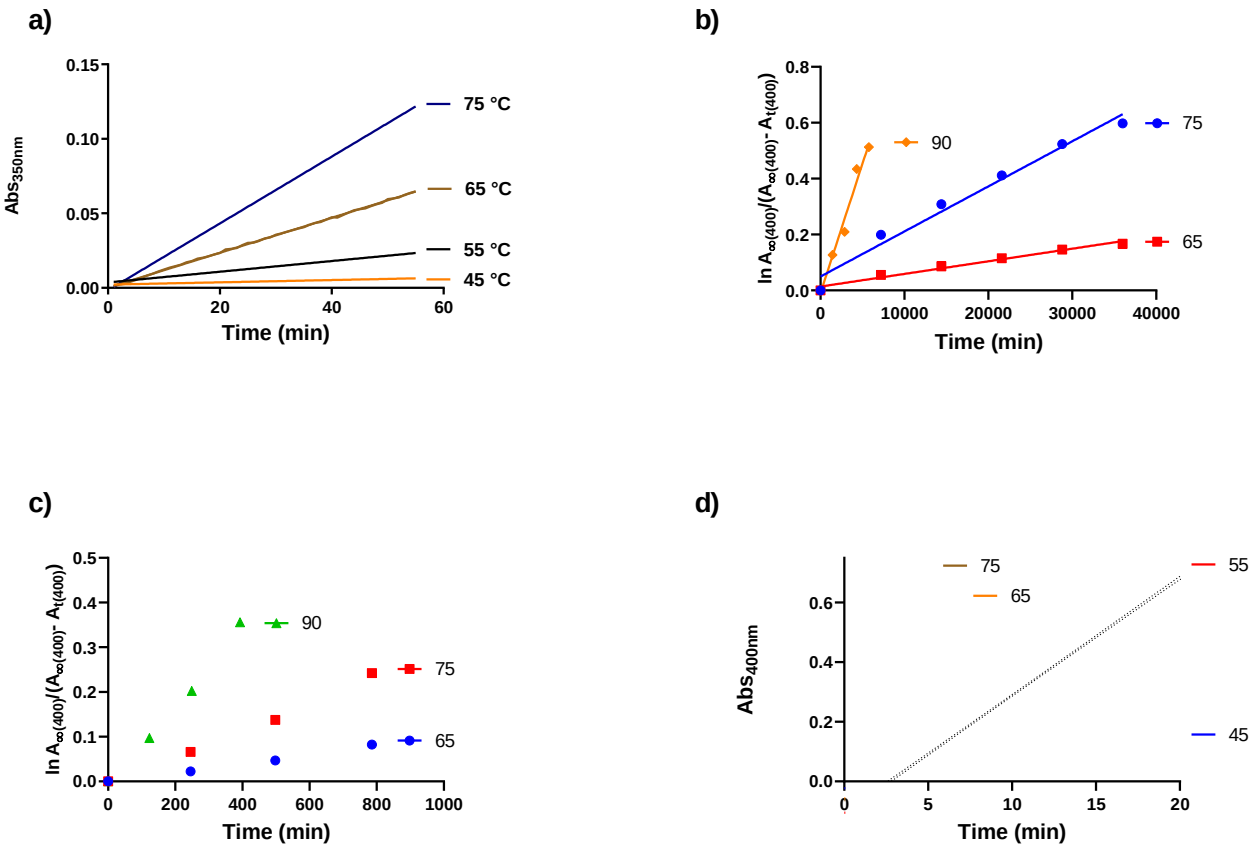

Figure S7. Plots showing formation of product versus time for at different temperatures for the hydrolysis of PNPGlc in acidic, pH-independent and basic regions.

a) Absorption-time curves at different temperatures in the acidic region in [HCl] = 1 M and 150 mM [NaCl], continuous assays at 350 nm. **b)** Absorption-time curves at different temperatures in the pH-independent region (pH 6.8) when [buffer] = 1 M stopped assays at 400 nm. **c)** Absorption-time curves at different temperatures in the weakly basic region (pH 8.4) stopped assays at 400 nm. **d)** Absorption-time curve at different temperatures in the strongly basic region in [NaOH] = 1 M continuous assays at 400 nm.

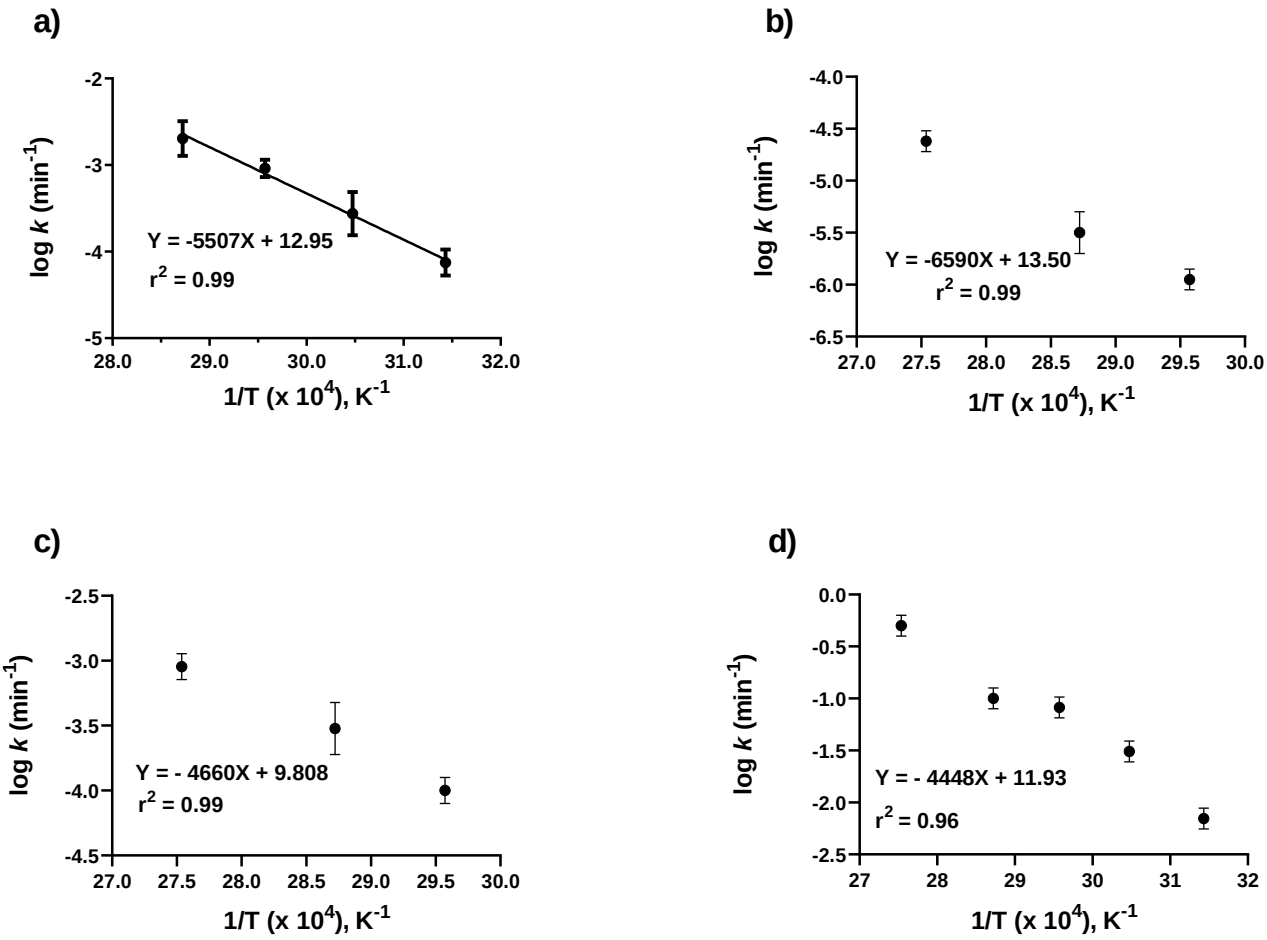

Figure S8. Arrhenius plots showing the relationship the hydrolysis rate constants of PNPGlc and inverse temperature 1/T (K^{-1}).

a) Plot in the acidic region. **b)** Plot in the pH-independent region. **c)** Plot in the weakly basic region. **d)** Plot in the strongly basic region.

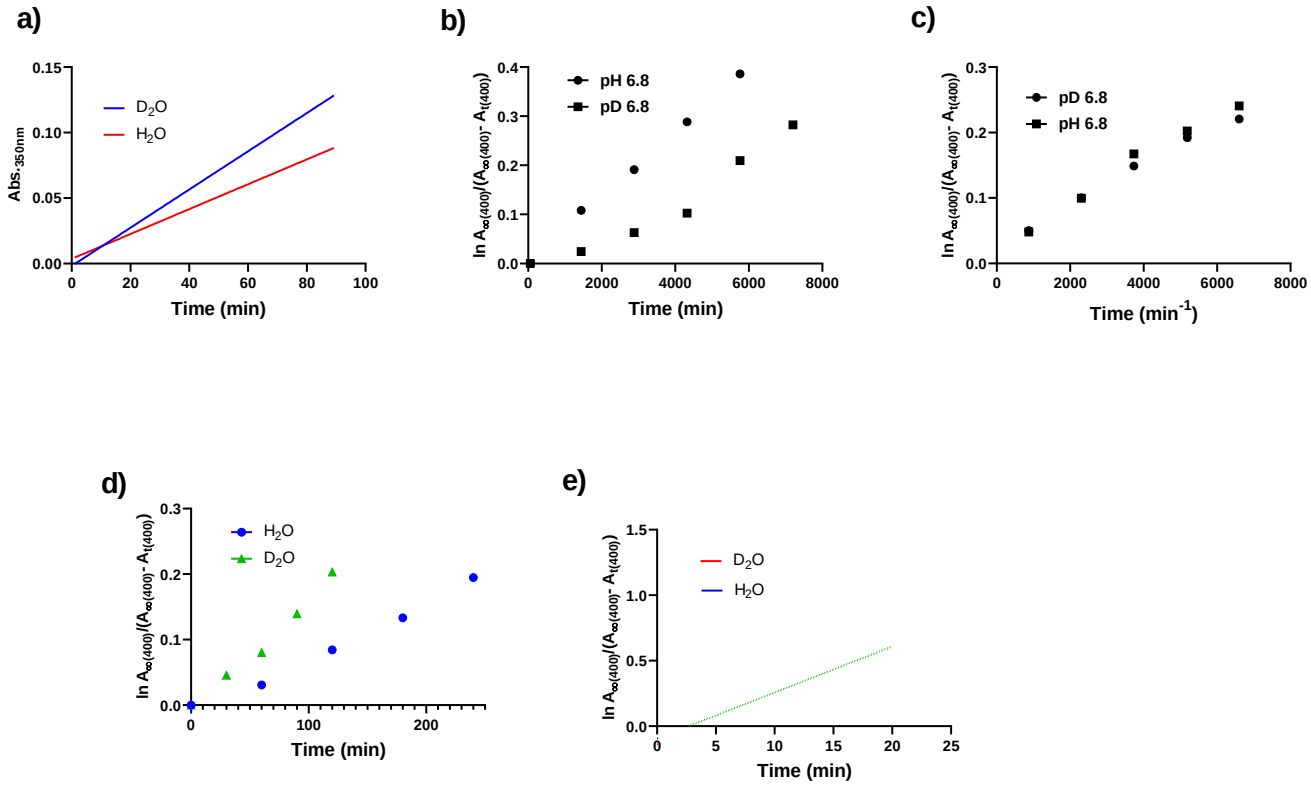

Figure S9. Plots showing formation of product versus time for solvent isotope effect (SIE) upon the hydrolysis of PNPGlc in acidic, pH-independent and basic regions.

a) Absorption-time curve for SIE in the acidic region (pH = pD = –0.75 at 75 °C, 150 mM [NaCl]) continuous assays at 350 nm. **b)** Absorption-time curve for SIE in the pH-independent region at 90 ^{o}C when [buffer] = 1 M stopped assays at 400 nm. **c)** Absorption-time curve for SIE in the pH-independent region at 90 °C when [buffer] = 5 mM (pH = pD = 6.8), stopped assays at 400 nm. **d)** Absorption-time curve for SIE in the weakly basic region (pH = pD = 8.4 at 90 °C), stopped assays at 400 nm. **e)** Absorption-time curve for SIE n the strongly basic region (pH = pD = 13.1) at 55 °C, continuous assays at 400 nm.

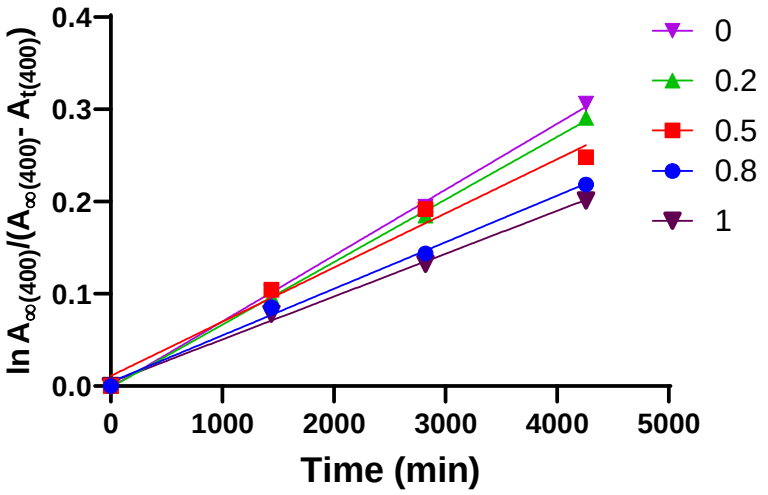

Figure S10. Plots showing formation of product versus time for proton inventory technique and the dependencies of the hydrolysis rate constants of PNPGlc on D_2O fraction (*n*) for the hydrolysis of PNPGlc in the pH-independent region p(H,D) 5.8 at 90 °C, [buffer] = 1 M.

a) Absorbance-time curve for the proton inventory technique in different fractions of D_2O, stopped assays measured at 400 nm.

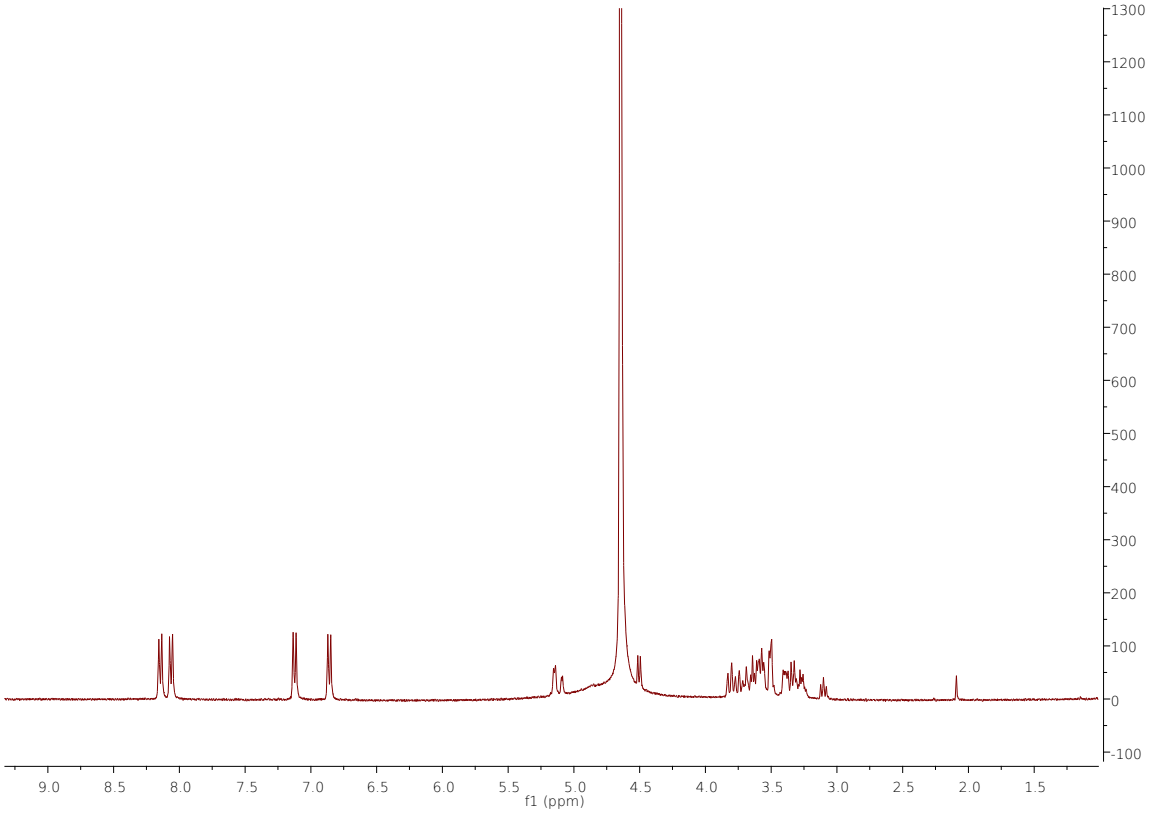

Figure S11. ^{1}H NMR spectrum of an aliquot after drying and redissolution in D_2O of the specific acid catalyzed hydrolysis of PNPGlc at 50% completion 75 °C, pH -0.8 (corrected).

(a)

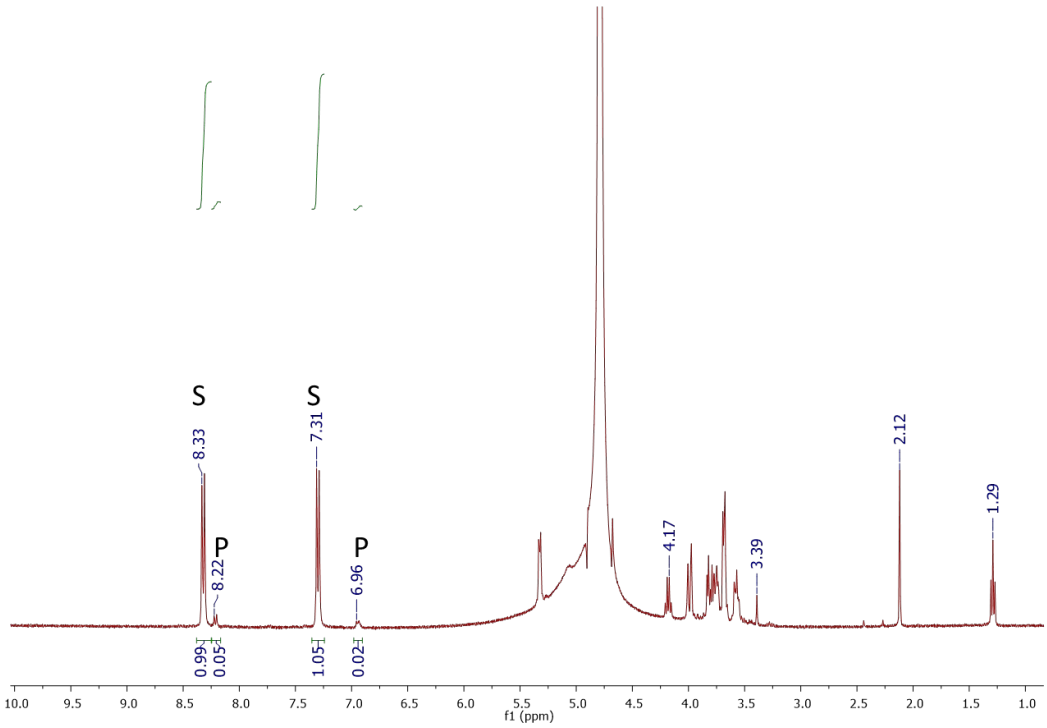

(b)

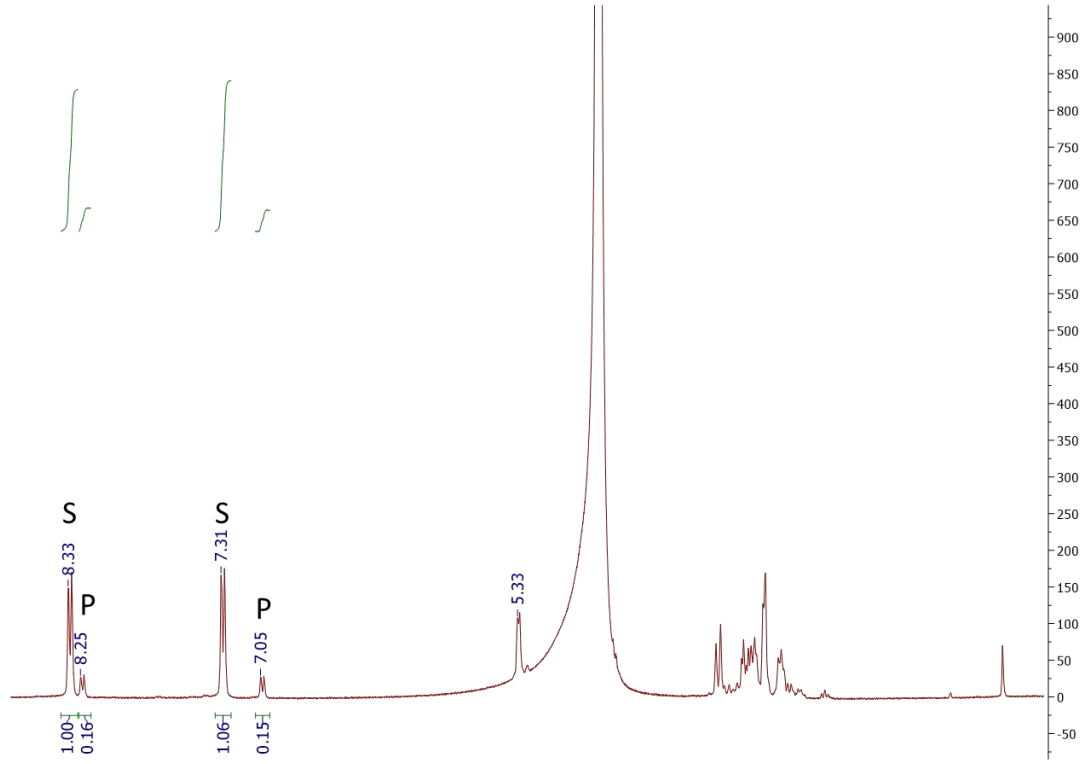

Figure S12. Representative ^{1}H NMR spectra aliquots after drying and redissolution in D_2O of the reaction of PNPGlc in the presence of 2 M $NaClO_4$ at 90 °C. **P** denotes the aromatic protons of the released PNP, **S** denotes the aromatic protons of PNPGlc.

a) time = 73 hours. **b)** time = 166 hours.

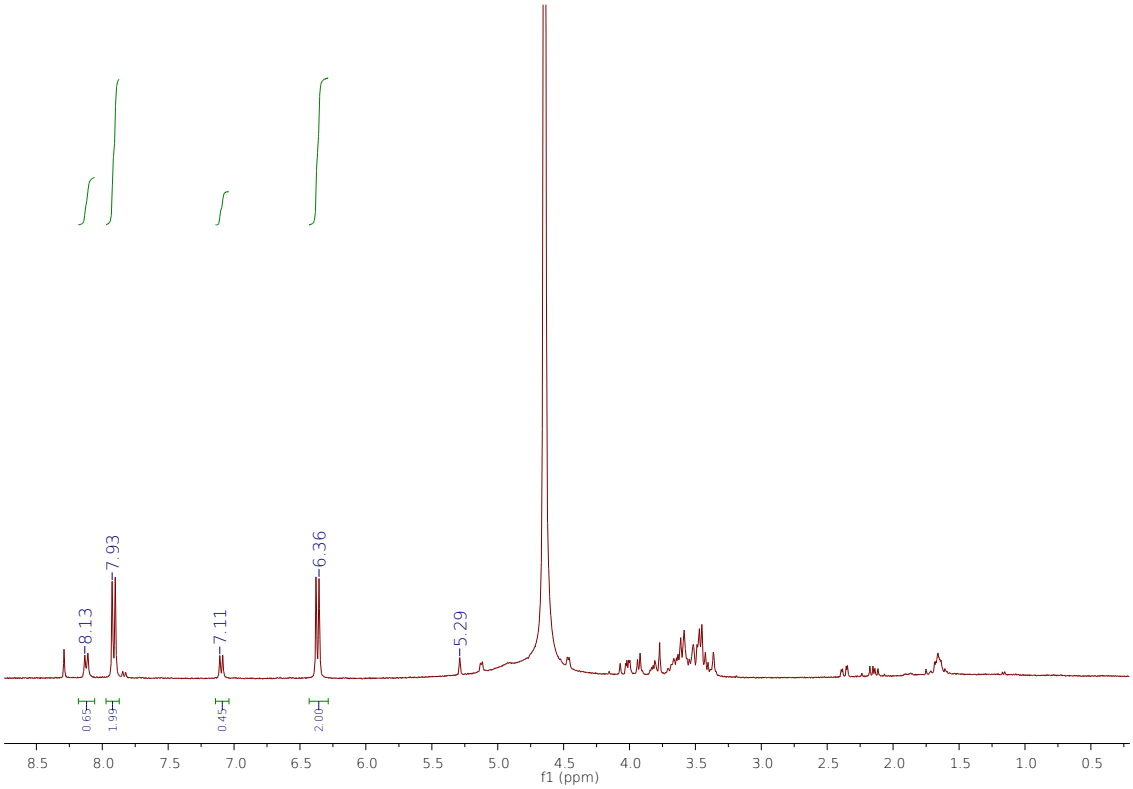

Figure S13. ^{1}H NMR spectrum of an aliquot after drying and redissolution in D_2O, of the reaction of PNPGlc in 1 M NaOH at 55 ^{o}C, showing formation of levoglucosan (δ 5.29 ppm).

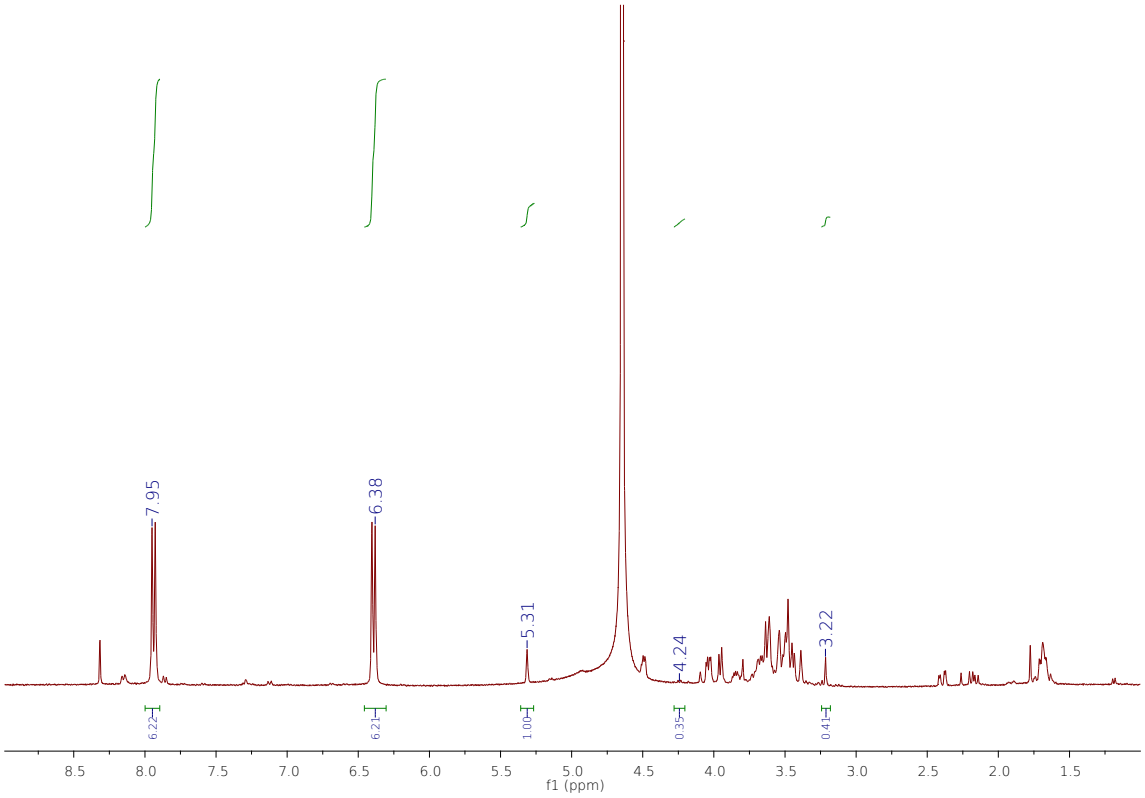

Figure S14. ^{1}H NMR spectrum of an aliquot after drying and redissolution in D_2O, of the reaction of PNPGlc in 1:1 MeOH/H_2O with 0.5 M NaOH at 55 °C.

Integration reveals the formation of methyl α-D-glucopyranoside, methyl β-D-glucopyranoside and levoglucosan in a ratio of 10:18:72.